CONTROL AND OPTIMIZATION OF CURE CYCLE FOR THICK-SECTIONED THERMOSET COMPOSITES MANUFACTURING

by

Özer Ünlühisarcıklı

B.S., Mechanical Engineering, Yıldız Technical University, 2005

Submitted to the Institute for Graduate Studies in
Science and Engineering in partial fulfillment of
the requirements for the degree of
Master of Science

Graduate Program in Mechanical Engineering
Boğaziçi University

2008

ACKNOWLEDGEMENTS

I would like to express my appreciation to my thesis advisor, Asst. Prof. Nuri Ersoy, who supported throughout my entire work, and my thesis co-advisor Prof. Eşref Eşkinat for his invaluable guidance.

I would also like to thank to the members of the evaluation committee, who have spared their valuable time for the assessment of this work.

I am very grateful to my friends, who gave me the motivation that helped me to finish this work. There are many names, and for the fear of leaving one out accidentally, I will not try.

Last but definitely not the least, I thank my family for their support and understanding.

ABSTRACT

CONTROL AND OPTIMIZATION OF CURE CYCLE FOR THICK-SECTIONED THERMOSET COMPOSITES MANUFACTURING

The objective of this study was to minimize the temperature gradients encountered in thick-sectioned thermoset composites manufacturing. For this purpose, a finite difference analysis based on mathematical models representing the curing phenomenon was developed. An optimization method, namely the sequential simplex algorithm was coupled with the analysis to minimize the temperature gradients.

A PID controller was developed in LabVIEW to allow the execution of cure cycles with arbitrary temperature profiles. An experimental setup was prepared, and experiments were carried out in order to check the consistency of the analysis with the experimental results.

Interpreting the experiment results, the efficiency of the approach was discussed, and potential ameliorations to the study were proposed.

ÖZET

KALIN KESİTLİ TERMOSET KOMPOZİT İMALATINDA KÜRLEME ÇEVRİMİNİN KONTROLÜ VE ENİYİLEMESİ

Bu çalışmanın amacı, kalın kesitli termoset kompozitlerin imalatında karşılaşılan sıcaklık gradyenlerini minimize etmektir. Bu gayeyle, kürleme fenomenini temsil eden matematiksel modellere dayanan bir sonlu fark analizi geliştirilmiştir. Sıcaklık gradyenlerini asgariye indirnek için bir eniyileme yöntemi, yani sıralı simplex algoritması analizle birleştirilmiştir.

Çeşitli kürleme çevrimlerinin uygulanabilmesi amacıyla LabVIEW programını kullanarak bir PID denetleyici geliştirilmiştir. Bir deney düzeneği hazırlanmış, ve analiz sonuçlarının deney sonuçlarıyla tutarlığını test etmek amacıyla deneyler yapılmıştır.

Sonuçlar yorumlanarak, sunulan yöntemin verimliliği tartışılmış, ve çalışmaya getirilebilecek iyileştirmeler önerilmiştir.

TABLE OF CONTENTS

ACKNOWLEDGEMENTS iii
ABSTRACT iv
ÖZET v
LIST OF FIGURES ix
LIST OF TABLES xii
LIST OF SYMBOLS/ABBREVIATIONS xiii
1. INTRODUCTION 1
1.1. Problem Statement 3
1.2. Literature Survey 6
1.2.1. Cure Control Strategies 6
1.2.1.1. Model Based Approach 7
1.2.1.2. Expert Systems 10
1.2.1.3. Alternative Approaches 11
1.2.2. Heat Transfer Model Dimensions 13
1.2.3. Sensing 14
1.3. Manufacturing Processes 17
1.3.1. Autoclave (Vacuum Bagging) Process 17
1.3.2. Compression Molding (Hot Press) Process 18
2. MATHEMATICAL MODELING 20
2.1. Thermochemical Model 20
2.1.1. Heat Transfer Model 20
2.1.2. Resin Cure Kinetics Model 21
2.2. Material Properties 23
2.2.1. Thermal Conductivity 24
2.2.2. Mass Density 25
2.2.3. Specific Heat Capacity 26
3. FINITE DIFFERENCE FORMULATION 27
3.1. Finite Difference Approximations 28
3.1.1. Forward Difference 28

3.1.2. Backward Difference 28
3.1.3. Central Difference 28
3.2. Finite Difference Methods 29
3.2.1. Explicit Methods 29
3.2.2. Implicit Methods 30
3.3. Application of the BTCS Method to the Problem 30
3.4. Boundary Conditions 33
3.5. Solution of the Equations 35
3.6. Computer Code for BTCS Method 38
4. CURE CYCLE OPTIMIZATION 39
4.1. Sequential Simplex Optimization Algorithm 39
4.2. Constraint Optimization. 46
4.2.1. Exterior Penalty Function Method 46
4.3. Application of the Method to the Problem 46
4.3.1. Objective Function 47
4.3.2. Design Parameters 48
5. EXPERIMENTAL SETUP 50
5.1. Hydraulic Unit 50
5.2. Heating Molds 52
5.3. Steel Frame 53
5.4. Working Principles 53
6. PID CONTROLLER DESIGN 55
6.1. The Basics of PID Controller 55
6.1.1. The Proportional Gain (K_P) 55
6.1.2. The Integral Gain (K_I) 56
6.1.3. The Derivative Gain (K_D) 56
6.2. Tuning the PID Controller 56
6.3. PID Controller in LabVIEW 58
7. RESULTS AND DISCUSSION 59
7.1. Analysis Results 59
7.2. Optimum Heating Profile 61
7.3. Experimental Results 63
7.3.1. Experiment #1 63

7.3.2. Experiment #2 64
7.3.3. Experiment #3 65
8. CONCLUSION AND FUTURE WORK 66
REFERENCES 68

LIST OF FIGURES

Figure 1.1. A typical cure cycle 2

Figure 1.2. Curing of a thermosetting resin 3

Figure 1.3. Effect of thickness on the midpoint temperature of USN 150 carbon fiber epoxy composite laminate 4

Figure 1.4. The results of an autoclave process conducted on a 25 mm laminate . . 5

Figure 1.5. Temperature profiles at the center of laminate obtained from one-dimensional and three-dimensional analysis 14

Figure 1.6. Diagram of omega heat flux sensor 16

Figure 1.7. Schematic of the autoclave molding process 18

Figure 1.8. Schematic of the hot press technique 19

Figure 3.1. Finite difference meshing 27

Figure 3.2. Stencil for the FTCS method 29

Figure 3.3. Stencil for the BTCS method 31

Figure 3.4. Representation of the heating setup 34

Figure 3.5. Finite difference mesh for half of the part 35

Figure 3.6. Flowchart of the FDA algorithm 38

Figure 4.1. Simplex geometries for 1-D, 2-D, and 3-D, respectively 40

Figure 4.2. Graphical representation of the operations 42

Figure 4.3. Flowchart of the Sequential Simplex algorithm 43

Figure 4.4. Contour map of Himmelblau's function 45

Figure 4.6. Calculation of the objective function 48

Figure 4.7. Representation of the cure cycle with discrete points 48

Figure 4.8. Representation of the cure cycle by a common time interval 49

Figure 5.1. Experimental setup 50

Figure 5.2. Schematic of the hydraulic circuit 52

Figure 5.3. The lower heating mold 53

Figure 5.4. Steel frame 53

Figure 5.5. Components of the experimental setup 54

Figure 6.1. The DC error 55

Figure 6.2. Overshoot caused by integral gain 56

Figure 6.3. Relay feedback system 57

Figure 6.4. Auto-tuning of the heating system 57

Figure 6.5. A sample performance of the controller 58

Figure 7.1. Analysis results for a 20 mm. part (MRCC) 60

Figure 7.2. Samples from the optimization progress 61

Figure 7.3. Optimum curing path for 20 mm. thickness 62

Figure 7.4. Experiment results for 10 mm. part (MRCC) 63

Figure 7.5. Experiment results for 20 mm. part (MRCC) 64

Figure 7.6. Experiment results for 20 mm. part (OCC) 65

Figure 8.1. Process times for individual phases 67

LIST OF TABLES

Table 2.1. Cure kinetics equations 22

Table 2.2. Cure kinetics constants 23

Table 8.1. Process times of individual phases 67

LIST OF SYMBOLS / ABBREVIATIONS

a	Size of the simplex
A	Cure rate coefficient
C	Diffusion constant
C_f	Specific heat capacity of the fiber
C_p	Specific heat capacity of the composite
C_r	Specific heat capacity of the resin
$\boldsymbol{e_k}$	Unit vector along the k coordinate
E_a	Activation energy
H_R	Total heat of reaction
k	Thermal conductivity
k_f	Thermal conductivity of the fiber
k_r	Thermal conductivity of the resin
k_t	Thermal conductivity in the transverse direction
K_d	Derivative gain
K_I	Integral gain
K_p	Proportional gain
K_u	Ultimate gain
m	First exponential constant
n	Second exponential constant
N	Number of design parameters
q	Heat generation
$\dot{q}$	Heat generation rate per volume
R	Universal gas constant
t	Time
T	Temperature
V_f	Fiber volume fraction
V_r	Resin volume fraction
x_0	Initial point
z	Through the thickness direction

α	Degree of cure
α_{CT}	Constant accounting for increase in α_C with temperature
α_{C0}	Critical degree of cure at T = 0 K
$\overline{\alpha}$	Thermal diffusivity
ρ_c	Composite density
ρ_r	Resin density
ΔT	Maximum temperature gradient

BC	Boundary Condition
DSC	Differential Scanning Calorimetry
FDA	Finite Difference Analysis
IC	Initial Condition
MRCC	Manufacturer's Recommended Cure Cycle
OCC	Optimized Cure Cycle
PID	Proportional-Integral-Derivative
RHS	Right hand side
RTM	Resin Transfer Molding
SUMT	Sequential Unconstrained Minimization Technique

1. INTRODUCTION

Materials science is one of the most important building blocks of the advancing technology. Throughout the history of humankind, it was the discovery of new materials that led our species to the next step in civilization. Even the eras are named after the material of that period (i.e. Stone Age, Bronze Age). Still, the engineers are striving for the development of advanced materials to answer the demanding needs of everyday life. Today, conventional engineering materials are basically grouped into three main classifications: metals, polymers, and ceramics. In addition, composites, semiconductors, and biomaterials constitute other groups of important materials.

In a composite material, two or more different types of materials are combined on a macroscopic scale to create a new material whose properties are superior to those of the original components. Even though composite materials existed in nature along with other natural materials, its production and utilization as an engineering material dates back to World War II (late 1940s and early 1950s) [1]. Recently, composite materials are being used in the industry at an increasing rate because of their superior properties to conventional engineering materials. They are generally preferred in weight sensitive applications like aerospace industry, due to their unique light-weight and high-performance features.

Fiber reinforced composites are generally manufactured in shell or plate form, due to their high inplane strength and stiffness. Also, conventional manufacturing processes are incapable of producing sound thick composite parts. These facts eventually limited composite materials' usage to thin-sectioned parts. Recent improvements in manufacturing techniques such as resin transfer molding (RTM) have rendered the manufacturing of thick-sectioned parts feasible. Recently, thick-sectioned composites are being used as components within bridge structures, tank and submarine hulls, and airplanes. However, many challenges still exist and there are many research areas yet to be studied regarding the manufacturing of thick-sectioned parts. One of these areas is the optimization of the cure cycle for better mechanical properties and shorter processing times.

Cure cycle may be defined as the time period in which the temperature of the part follows a defined profile over time. In some manufacturing processes, such as vacuum bagging process, pressure and vacuum may be applied as well. A typical cure cycle consists of increasing the temperature to a set point at a specific rate, holding the temperature until the part has cured to a reasonable extent, and then cooling the part to ambient temperature. Generally, an earlier dwell is applied when thermosetting composites are considered. Figure 1.1 represents a typical cure cycle, with two hold temperatures. The first dwell is intended for the proper consolidation of the laminate and the second dwell is for the curing of the matrix. There are several critical factors regarding the determination of the cure cycle, which will be discussed later on.

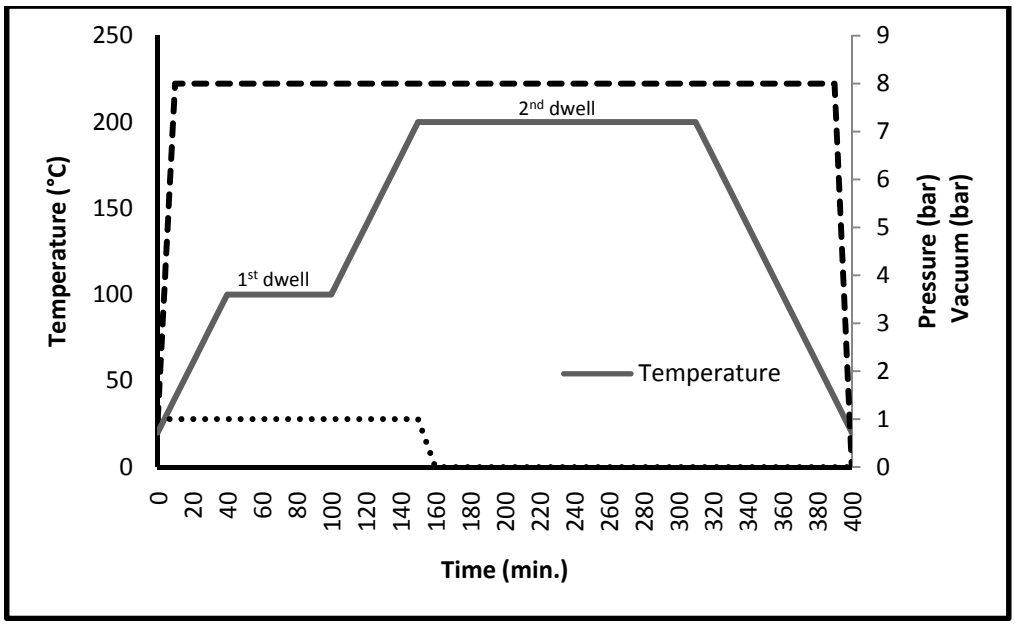

Figure 1.1. A typical cure cycle

Curing (polymerization and cross-linking terms are also used interchangeably) is a complex series of chemical reactions which takes place in thermosetting polymers. Initially, a thermosetting resin is in liquid state at room temperature. When subjected to heat (and proper catalysts in some cases) the curing reaction is initiated. During the curing of a thermosetting resin, the molecular chains composing the polymer form a three-dimensional cross-linked network, which adds strength and rigidity to the material. This is a one-way reaction – once cured, thermosetting materials cannot be melted or reshaped. A schematic representation of the curing reaction is presented in Figure 1.2.

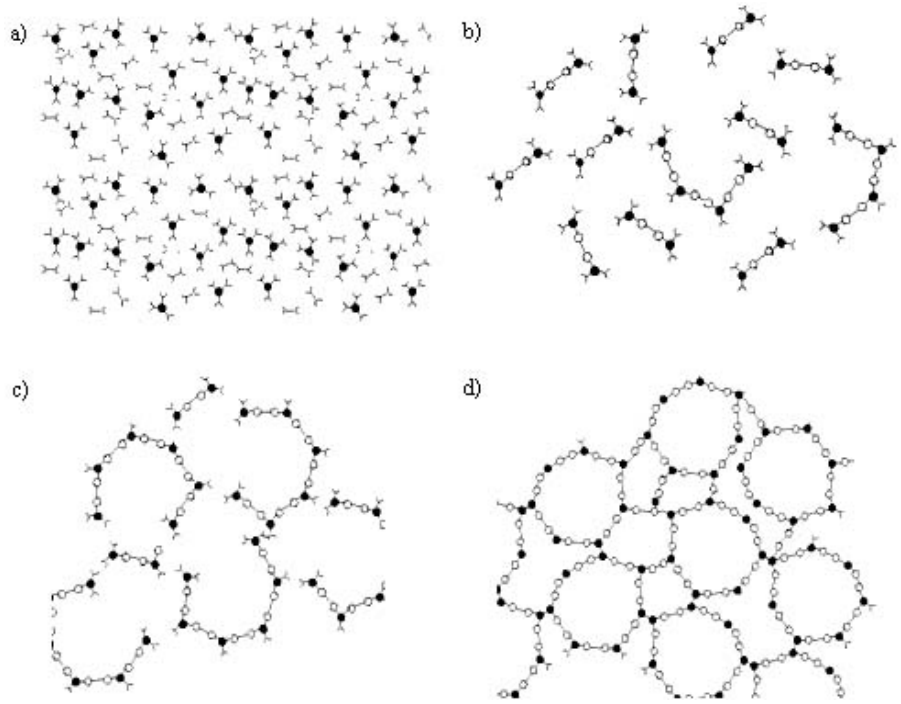

Figure 1.2. Curing of a thermosetting resin: a) monomer stage, b) linear growth and branching, c) formation of gelled but incompletely cross-linked network, d) fully cured thermoset [2]

1.1. Problem Statement

In composites manufacturing, the strength and shape of the finished part is highly sensitive to processing parameters. For instance, insufficient consolidation causes poor bonding between composite layers. A slight deviation from the optimal heating rate results in reduced mechanical properties. Overheating may cause delamination or even polymer degradation. Maybe, the most important one of these parameters is the temperature distribution throughout the part. During the curing stage of composite laminates, the temperature distribution should be uniform throughout the part in order to avoid residual stresses and distortions in the part geometry. While working with thin laminates (thickness less than 5 mm), the heat diffuses rapidly and the temperature distribution is sufficiently uniform [3]. Most composite materials manufactured thus far were thin plates or shells and thus temperature uniformity was not an issue. However, in thick sectioned composite parts, if not controlled, thermal gradients throughout the part become significant, and should be avoided. The mechanics behind this phenomenon is explained below.

The heating of the part is performed by heaters which are positioned close to the part surface. In the early stages of curing, the outer surface temperatures are somewhat higher than the central temperature, as it takes some time for heat to diffuse into the part (the matrix is composed of some type of polymer, which inherently possesses a low thermal conductivity). The magnitude of this temperature difference depends on the temperature ramp. Above a critical temperature ramp, the outer surface temperature rises a lot more than the internal temperature. This eventually causes outside-inside curing which is unfavorable, because of void formation [4]. However, an unnecessarily slow heating rate is also undesirable because of manufacturing cost considerations.

The second stage of curing shows an exactly opposite behavior. The polymerization of thermoset polymers is an exothermic reaction. While the cross-links form, the double bonds between the molecules break down [5], generating heat at the same time. As the cure progresses, the heat generated by the exothermic reaction gets entrapped inside the composite, initiating an autocatalytic chain reaction. The internal temperature rises above the surface temperature, causing inside-out curing. Although inside-outside curing is preferable to some extent [6], uncontrolled curing may cause uneven curing, which eventually causes residual stresses and shape distortions in the part. The severity of this effect grows with increasing thickness, as can be observed from Figure 1.3.

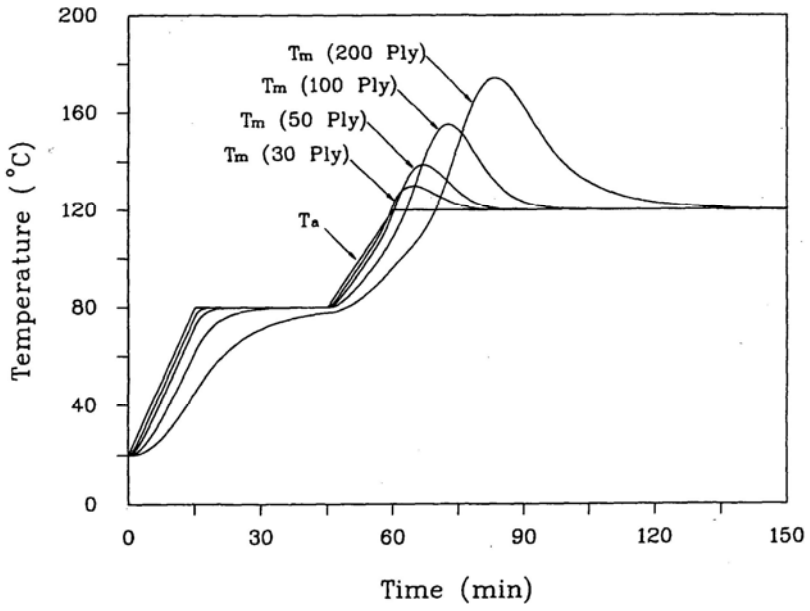

Figure 1.3. Effect of thickness on the midpoint temperature of USN 150 carbon fiber epoxy composite laminate [7]

This is actually a common problem encountered in the composites industry. For example, Figure 1.4 shows the experimental data obtained from an undisclosed airplane components manufacturer. Although the heaters are turned off as soon as the autoclave temperature reaches 180 ºC (which is the curing temperature of the composite), the internal temperature continues to rise up to 214 ºC because of the reaction energy. Therefore, precaution should be taken before the system reaches the point of no return.

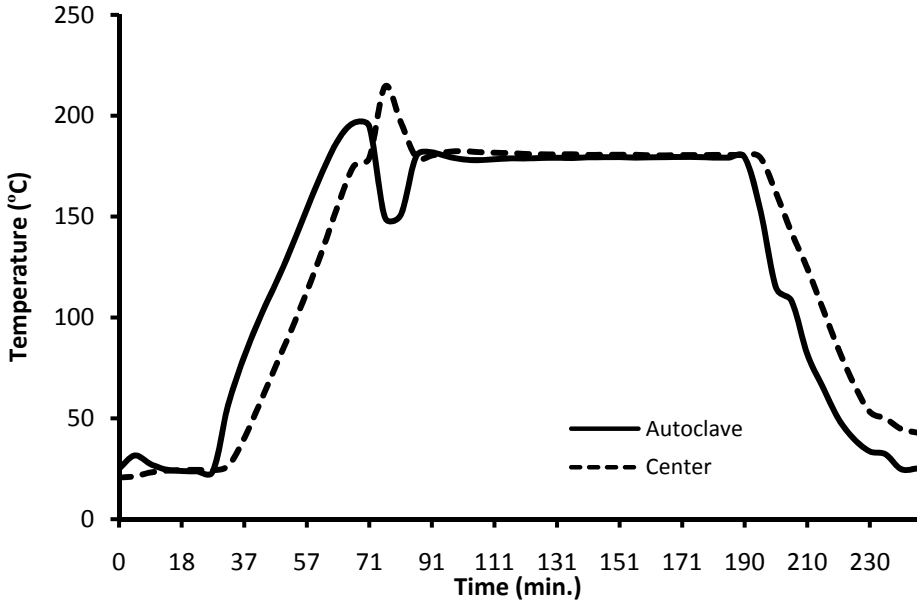

Figure 1.4. The results of an autoclave process conducted on a 25 mm laminate

The thermal gradients can be minimized by heating the part at a lower rate. But, this results in longer processing times, which in return increases production costs. This conflict encountered in both of the cure stages can be considered as a constrained optimization problem, which minimizes the cycle time while keeping the thermal gradients within specified limits.

For thin-sectioned parts, the optimal cure cycle for the composite is generally supplied by the manufacturer, which is referred as “Manufacturer’s Recommended Cure Cycle” (MRCC). Determination of the MRCC is usually based on a trial-and-error approach. Although this approach is considered effective for thin parts, it turns out to be very expensive or even inapplicable due to the complexity of the problem. Different approaches to the solution of this problem are presented in the following section.

1.2. Literature Survey

The subject of curing of thick-sectioned thermosetting composites has attracted the attention of many researchers. Numerous studies have been conducted on this interesting subject. This review will briefly describe the previous research.

While some of the researchers concentrated merely on inspecting the curing phenomena either by experiments and/or simulations, others also utilized optimization algorithms in order to improve process quality. These studies basically differ from one another by the proposed cure control approach and the optimization scheme, the extent of the mathematical model, and the sensors implemented for process control and monitoring.

1.2.1. Cure Control Strategies

Until the development of computer-based numerical methods, the cure cycles for thick-sectioned composites were determined by a trial-and-error procedure [8]. While still being the primary method for the determination of conventional cure cycles, trial-and-error method is costly, time consuming and non-optimal for thick-sectioned parts. The introduction of computers provided us with new means of cure control. These strategies can be divided into two main categories: “Model based” approach in which a simulation is performed to determine an optimal cure cycle before the process begins, and knowledge-based “expert systems” in which the process is modified according to the input from the sensors during the process. The latter method is based on a set of rules such as “IF the thermal gradient is greater than 10 °C, THEN turn off the heaters”. Each method has its characteristic advantages and disadvantages. The former method requires a non-linear control algorithm, extensive computational power, and an accurate model of the whole process. The accurate modeling of batch processes is questionable because of the batch-to-batch variations, the change of physical and thermal properties during the process, and other unpredictable factors. On the other hand, while the second method is much more simple, it cannot predict what is to come, and may not deal with the sudden heat released from the autocatalytic reaction. In addition, expert systems have not yet been tested for parts with complex geometries [5].

1.2.1.1. Model-Based Approach. In model-based approach, a simulation is carried out based on a mathematical model which defines the whole process. The accuracy of the simulation is a major concern in model-based approaches. The highly heterogeneous nature of the batch processes causes uncertainties in the model. Also, the cure kinetic models developed thus far are generally semi-empirical models which cannot provide exact characterization of the process. Cure modeling will be investigated in detail in Chapter 2.

The model representing the process is a non-linear differential equation due to the coupled nature of the thermal and chemical phenomena which take place during curing. The solution of this non-linear model is another issue. The model should either be solved by finite difference, finite element or some other numerical method and requires extensive computational power. Also, the assumptions made for rendering the problem solvable (like constant thermal properties, 1-D heat transfer, etc.) add further to the inaccuracy of the model. It is unnecessary to emphasize on the difficulties of optimization and control of non-linear model-based processes.

One of the preliminary studies about the modeling of curing was conducted by Loos and Springer [9] in 1983. They developed their model in four parts: “Thermo-chemical model” which yields the temperature, the degree of cure, and the viscosity; “flow model” which yields the pressure, the resin flow out of the composite, and the resin content of the composite and the bleeder; “void model” which yields the void size and the temperature and pressure inside the void; and finally “stress model” which yields the residual stresses. Experiments were performed for the verification of thermo-chemical and resin flow models. By changing the processing parameters in the simulation, they inspected the effects of different cure cycles on the part quality. Although they suggested that this parametric approach could be used for the determination of improved cure cycles, they did not implement any numerical optimization scheme. Anyways, the study carried out by Loos and Springer set the ground for future researchers [10].

As previously stated, one way of reducing the thermal gradients is to apply a slower heating rate. This approach is successful in producing sound parts, but at the expense of increased manufacturing time and cost. As a different attempt, Kim and Lee [7] developed an autoclave cure cycle including cooling and reheating steps which effectively cured 15

mm and 30 mm thick carbon fiber epoxy composite laminates without increasing the processing time. The cooling mentioned above actually refers to the cooling of the autoclave. Even if the temperature of the autoclave drops, temperature in the middle still rises because of the heat generation. The cooling type was not a forced cooling, due to the lack of a computer controlled cooler. Such a setup might further increase the success of the cooling and reheating approach. The drawback of this method is that it focuses on preventing the temperature overshoot inside the part; however it does not take the thermal gradients into account. As the autoclave temperature drops, surface temperature drops as well, while inner temperature continues to rise. Actually, thermal gradients up to 20 °C may be observed. It should also be noted that the simulation over-predicted the middle temperature about 10 °C. The authors relate this discrepancy to the assumption of constant thermal properties, and to the possible inaccuracies in the kinetic model.

Oh and Lee [11] conducted a comprehensive study for the optimization of cure cycle of thick glass/epoxy laminates. The temperature gradient phenomenon occurs more severely when glass reinforced polymers are considered, due to even lower thermal conductivity of glass fibers. Their three-dimensional finite element analysis including resin flow showed very good agreement with the experimental results. The optimization process was composed of two steps. The first step was the determination of the minimum time required for the full consolidation of the laminate. The resin flow included in the analysis forms the basis of this step. Three-dimensional analysis shows far better results than one-dimensional case when resin flow is considered. This is because the permeability of the prepreg in the fiber direction is much higher than the transverse direction, thus the fiber direction should also be included in the model. In the second stage, cooling and reheating steps were introduced to prevent the temperature gradients, much like the method proposed by Kim and Lee [7]. The constrained optimization problem was reduced to an unconstrained problem by the introduction of penalty functions and a Sequential Unconstrained Minimization Technique (SUMT) was used at each iteration. It was found out that the method prevented the large temperature gradients without increasing the processing time.

Yang and Lee [12] developed a method which uses the knowledge from conventional curing process of thin laminates to determine the curing cycles for thick laminates.

Conventionally, cure cycles of thermosetting composite laminates are primarily determined by using trial-and-error methods. Although trial-and-error approach is cost effective for thin laminates, it is not desirable for thick-sectioned parts due to the high cost of the experiments. Yang and Lee claim that by using the parameters obtained from the curing of thin laminates, they have reduced the curing cycle with no difference in the interlaminar shear strengths in a cost-effective way. Unfortunately, the cure cycle they compare with is an extended cure cycle, which is 2.5 times of a cure cycle for a thin laminate. Actually, they preserve the mechanical properties by extending the cure cycle by 66.6%. Furthermore, the only parameter they modify is the dwell time.

Residual stresses also can have a significant effect on part quality by inducing warpage, micro cracks, and delaminations. The sources of process-induced residual stresses include ply anisotropic thermal expansion, anisotropic resin cure shrinkage strains, cure and temperature gradients, tooling effects, and internal resin flow. By applying a proper cure cycle, the effect of cure and temperature gradients on residual stresses can be minimized. In the early studies conducted on residual stress development, only stresses caused by ply anisotropic thermal expansion in the cool down stage were considered [13]. The first to study residual stress evolution in thick-sectioned composite laminates throughout the whole process cycle were Bogetti and Gillespie [14]. They developed an incremental laminated plate theory model which is coupled to a one-dimensional cure simulation analysis. The one-dimensional model used in this study is a simplified version of the two-dimensional model previously developed by Bogetti and Gillespie [4]. Temperature and degree of cure distribution obtained from the cure simulation was incorporated into material models to predict cure dependent material properties. Namely, resin modulus, resin chemical shrinkage, composite mechanical properties, composite chemical shrinkage strain, and composite thermal expansion strain. Then, these properties were used as input to the classical laminated plate theory based stress model. According to the experiments, the specific volume change caused by thermal expansion, and cure shrinkage was shown to be important sources of internal loading. Also it was shown that the moment when the resin modulus begins to develop has a significant effect on process-induced residual stresses.

1.2.1.2. Expert Systems. Another approach to the cure control is to use knowledge based expert systems. As previously discussed, the issue with model based approach is that it requires an accurate numerical model of the whole process. On the contrary, the expert system approach does not require any mathematical model or data regarding the material properties. Instead, the process is modified online according to pre-determined rules of thumb (or heuristics). However, they do not provide a generalized method. The rules embedded in the expert system are very process specific. Even a slight modification in the process parameters might require extensive research.

Ciriscioli et al. [15] adopted an expert system which combines the sensory data directly with a set of rules which are expressed as conditional statements. The data acquired from the sensors are directly evaluated by a series of IF … THEN statements, like "IF degree of cure is above x, THEN turn off the heaters". Their control system takes into account not only temperature gradients but also the compaction, residual stresses, and voids generated during the curing process. The monitored properties during the cure were the autoclave temperature, surface temperatures of the composite, midpoint temperature of the composite, dielectric properties inside the composite, thickness of the composite, and autoclave pressure. These data were used as an input for the control system designated as SECURE, and the autoclave temperature and pressure were controlled accordingly. The experiments resulted in reduced cycle times, while the mechanical properties remained the same when compared to conventional processing methods. However, the method does not rely on any mathematical model, so the sudden rises in internal temperature, due to the exothermic curing reaction, cannot be estimated beforehand. This might result in high temperature gradients and material degradation under different conditions.

Pillai et al. [16] developed a hybrid method which augments the model based approach with a knowledge-based system. The optimal temperature profile obtained using the mathematical model was implemented using an expert system. Due to the complexity of the problem, the aim of the optimization was only to obtain a near-optimal profile. This was achieved by using an optimization algorithm called "local criterion optimization". It is a dynamic programming approach which assigns a discrete set of values to the controlled variable (which is temperature in this case), and evaluates the results of these selections using a heuristic-based approach. In contrast to the previous studies that directly apply the

optimal trajectory, Pillai et al. used a "process trend analysis" (PTA) strategy to compensate for the discrepancies between the simulated process and the actual process. Implementing the optimal profile obtained using a mathematical simulation with an expert system is a very robust approach. Using this system, it is possible to optimize a process even if the process model is inexact. However, the optimal profiles obtained by local criterion optimization lead to a traditional two-ramp cure cycle. In other words, the optimization method discards any cure cycle other than the two-ramp structure.

1.2.1.3. Alternative Approaches. The alternative methods used for manufacturing of thick-sectioned composites are discussed below.

White and Kim [17] developed a technique called "staged curing" which is especially suited for the manufacturing of thick-sectioned composites. This technique consists of two interrupted curing stages. In the first stage, relatively thin layers of material are subjected to a consolidation cycle, and then cooled down to room temperature. Subsequently, a second stack is placed on top of the first, and the whole stack is subjected to the same consolidation cycle. This procedure is repeated until the desired thickness is achieved. At the end of this stage, proper consolidation is achieved (because the consolidated part is relatively thin), and some of the stored exothermic energy is released. Additionally, the cooldown of the part after consolidation but before gelation causes shrinkage and collapse of voids. In the second stage, the whole thick-sectioned part is subjected to a dwell at cure temperature. Since some of the exothermic energy has been released in the first stage, there is less energy available for thermal spiking. Mechanical tests carried on double cantilever beam specimens and interlaminar shear strength specimens showed that no degradation occurred in mechanical properties. Moreover, micrographs of the stage cured parts demonstrate a significant reduction in void content. However, the tests were conducted only on 2.6 mm thick specimens, and there is no guarantee that this method will be efficient for thicker sections. Furthermore, the requirement of an additional consolidation cycle for each subsequent layer increases the cycle time excessively. The MRCC for the AS4/3501-6 graphite/epoxy used in the study is 300 minutes. A four stacked cure cycle would take approximately 850 minutes until complete curing of the part, which is almost three times the MRCC.

Pre-catalyzing fabric is a promising method proposed by several researchers [5, 18]. In the first stage of this method, the fibers are ‘sized’ with the catalyst using a binder material. After the resin is applied on the pre-catalyzed fibers, the binder begins to dissolve and the catalyst starts to diffuse into the resin. This initiates the free radicals, causing free radical polymerization. Unlike conventional systems, the speed of the reaction depends on the rate of diffusion of the catalyst into the resin. As a result, the polymerization reaction is much less violent. Reuss et al. [18] examined this method for manufacturing two different combinations. First method uses polystyrene as the catalyst binder and toluene as the solvent, the second method uses epoxy as the binder and acetone as the solvent. After a set of experiments, it was concluded that using the epoxy binder had advantages over polystyrene to improve the cure degree. Unfortunately, pre-catalyzing fabric method cannot be applied to prepreg materials because in a prepreg material the fibers and the fabric are already bonded to some extent. Still, pre-catalyzing fabric method provides a good alternative to pre-mixing method.

Microwave curing has been considered as an alternative to thermal curing for a long time, but it has not gained acceptance in the field yet, probably due to the requirement of equipment and special tooling [19]. Realizing the potential of microwave curing and the lack of an analytical model, Lee and Springer [10] studied the response of thermosetting composites subject to electromagnetic radiation. They developed a thermochemical model which involves radiation heat transfer, and then coupled this model to the flow, void, and stress models previously developed by Loos and Springer [9]. The experiments showed that the microwaves penetrated only glass fiber reinforced composites or unidirectional graphite fiber reinforced composites. Also, the fact that the microwaves might affect the polymer structure of the matrix was not considered in the study.

Ramakrishnan et al. [20] explored the effectiveness of internal resistive heating provided by conductive carbon mats embedded inside the part. In this method, the carbon reinforcement has a heating function as well. This is performed via applying a DC voltage across the carbon fibers. Although this method sounds brilliant at first, it has several issues. The localized heating within the part causes excessive void formation as the volatile components in the matrix vaporizes. Additionally, although the global thermal gradients

are reduced, local gradients still exist due to the localized heating. Also, it is obvious that the use of this method is limited to carbon fibered composites.

1.2.2. Heat Transfer Model Dimensions

All heat transfer models found in the literature use a variation of Fourier's transient heat conduction equation with a heat generation term. The majority of these models consider heat conduction only in through-the-thickness direction (one-dimensional model) [7, 9, 10, 14]. This approach is sufficiently accurate if planar dimensions (x and y) are very large when compared to the thickness of the part. A "lumped" or zero-dimensional model would be much simpler; however, it is only applicable to very thin parts which have the same temperature at every point, and remains out of the scope of this study.

Two and three-dimensional models that allow heat transfer in more than one direction also exists. In one of the earliest studies on the subject, Bogetti and Gillespie, Jr. [4] based their cure simulation model on a two-dimensional, transient anisotropic heat transfer analysis. An incremental, transient finite difference solution was implemented to solve the governing equations. Along with a generalized boundary condition formulation, the two-dimensional cure simulation allows the study of arbitrary cross-sectional geometries. Two-dimensional approach is applicable if at least one dimension is much larger than the other two (e.g. x >> y and z) [13]. This model assumes that temperature gradients are significant only in the modeled plane, such as in hat sectioned parts. Park and Lee [21] also developed a two-dimensional cure simulation, applying the finite element method. When compared to the solutions based on the finite difference method, the finite element method allows the modeling of complex geometries more accurately, like the mandrel used in a filament winding process. Choi et al. [22] carried out three-dimensional simulations of curing in the RTM process. A three-dimensional model allows the study of any geometry, but greatly increases the computational cost of the problem.

Oh and Lee [11] compared the accuracy of one-dimensional and three-dimensional simulations for an autoclave process. As can be seen from Figure 1.5, the two simulation curves are almost coincident except the slower cooling rate of the one-dimensional simulation after the temperature overshoot. The authors relate this difference to the fact

that in the one-dimensional analysis, it is assumed that heat is transferred only from the top and bottom surfaces, whereas three-dimensional simulation also allows the heat transfer from the edges. It should be noted that this comparison was made for a flat plate with the dimensions of 100 mm x 100 mm x 20 mm and is not valid for complex geometries.

It is obvious that the more dimensions considered in the model, the higher the accuracy. However, the slight increase gained in accuracy should be compared with the extra computational effort required. The assumption of one-dimensional heat transfer allows for a simpler model and faster simulations. As our study will only focus on flat plates with large planar dimensions, using a one-dimensional model will be more efficient.

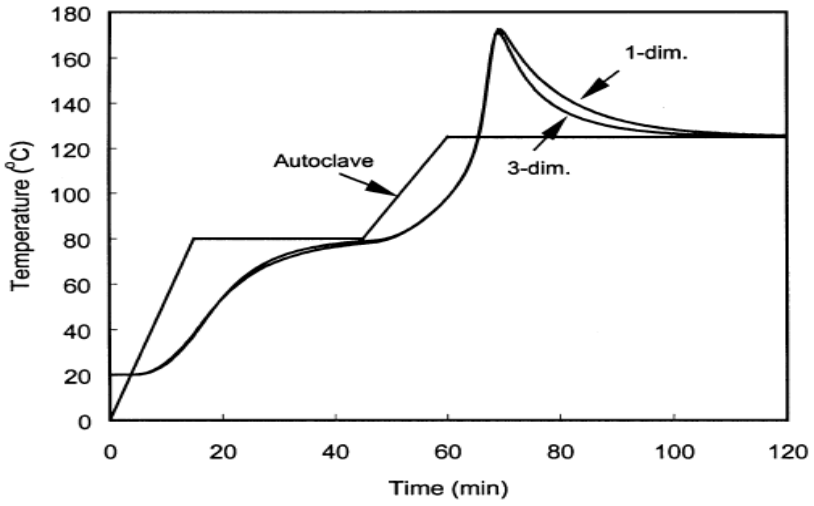

Figure 1.5. Temperature profiles at the center of laminate obtained from one-dimensional and three-dimensional analysis [11]

1.2.3. Sensing

The data provided by the sensors are essential for the control of composites manufacturing process. The accurate control of the process would not be possible without a sensor measuring the mold temperature. In addition to the mold temperature, one might find the need to measure the internal temperature, heat flux through the part surface, or any other material property such as degree of cure of the resin. The sensors used in cure control may be classified as “intrusive sensors” and “non-intrusive sensors”. Intrusive sensors are placed inside the material and remain there after processing. Although the in-situ

measurement of the internal properties of a composite laminate is desirable, intrusive sensors have certain drawbacks in practice. Once the matrix has cured, there is no way of dismounting the sensors without damaging the part. Certainly, a part which will be used in real-life applications should not bear any sensors embedded inside. And even for experimental purposes, it has to be kept in mind that the presence of intrusive sensors compromises the part strength. Thus, test specimens should be prepared from sensor-free regions. Obviously, intrusive sensors are not reusable. On the other hand, non-intrusive sensors do not suffer from these drawbacks. However, such sensors' distance from the center of the part arises questions regarding their accuracy about the internal behavior.

Thermocouples have been the most preferred sensor due to their low cost, ease of installation, and versatility. They can be used outside the part to measure the mold temperature, or they can be embedded within the laminate to measure internal temperature. The internal temperature of the laminate provides a great deal of knowledge about the process. Other material properties such as viscosity, degree of cure, etc., can be derived from temperature measurements using cure kinetic models. Additionally, a peak in internal temperature may indicate the beginning of curing, or the stabilization of the temperature may indicate that the curing is over. Although thermocouples are the easiest to use, they have the drawbacks of intrusive sensors discussed above.

Instead of relying on internal thermocouples that compromise part strength, Michaud et al. [23] used non-intrusive heat flux sensors measuring the amount of heat being transferred into or out of the composite. Two sensors are placed on the top and bottom surfaces of the mold, measuring the heat flux passing across the boundary. A heat flux sensor has several thermocouple junctions on either side of a thin polyamide film barrier (Figure 1.6). The thermal gradient across the barrier is directly proportional to the heat transfer rate [23]. Heat flux sensors allow the direct measurement of energy release independent of the thermal mass of the system. However, the usage of heat flux sensors is problematic in situations where there are more than one heat source, such as the heat generated by the heaters and the heat released from the exothermic reaction. Also, heat-flux sensors do not have a long service life; their performance deteriorates in time.

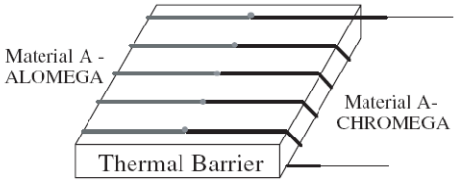

Figure 1.6. Diagram of omega heat flux sensor [23]

Pantelelis [24] based the real-time monitoring of the material state on dielectric measurements. Dielectric cure monitoring systems actually measure the conductivity of the ions within the resin, which tend to migrate towards the opposite polarity. The migration speed of these ions is related to the viscosity of the resin. As cross-linking proceeds during curing process, the viscosity of the resin increases, resulting in a reduction in the migration rate [25]. The viscosity and degree of cure of the resin can be determined from the dielectric measurements. However, the difficulty in relating the sensor measurement to the resin mechanical properties, and the requirement of a good contact between the sensor and the composite while isolating from the conductive fibers should be kept in mind when selecting this type of sensor.

Parthasarathy et al. [3] preferred a non-linear observer design to intrusive sensors that remain embedded in the part, throughout its lifetime. An observer is an estimate of missing information regarding the system, based on a mathematical model. The observer developed by Sanjay et al. uses the surface temperature as an input, and estimates the internal temperature using a mathematical model of the system. Embedded sensors may be considered acceptable for research purposes, but non-invasive techniques are indispensable for real-life applications.

Fiber optic sensors provide a versatile alternative for process monitoring. Their immunity to electromagnetic fields, electrical isolation, and small size make them superior to common sensory devices. In fact, these tiny sensors can be embedded inside the part without significantly effecting its mechanical properties. Antonucci et al. [26] used a unique fiber optic sensor integrating a refractometer and a fiber Bragg grating for monitoring the consolidation of a thermoset resin. The method relies on the measurements of the optical properties of the resin, which changes as the chemical reactions advance. The optical properties measured by the refractometer gives an idea about the degree of cure by

the use of Lorenz-Lorentz law which relates the refractive index to the density of the resin. The fiber Bragg grating is used for the measurements of process-induced strains, using a relation between strain and the Bragg wavelength shift. The experiments show that fiber optics is a promising technique in cure monitoring.

The thermal properties of thermoset resins are difficult to define during processing, due to the presence of internal heat generation and the double dependence of the thermal properties to temperature and degree of cure. Garnier and Sommier [27] proposed a method for measuring the thermal properties by using steady periodic conditions. They separate the heating effects of the exothermic reaction by applying a sinusoidal heating and eliminating the non-periodic components from the sensor output by high-pass analog filters. They use a quasi isothermal mode to obtain the effects of the degree of cure on thermal diffusivity. This way, they separate the effect of the temperature on thermal diffusivity from that of the degree of cure. Although this method might prove to be useful for determining thermal characteristics, it is not applicable to real manufacturing processes because of its sinusoidal heating conditions and other complexities.

This section covered some of the approaches in the literature. Until now, none of these approaches proved to be the widely accepted, standard method for manufacturing thick-sectioned composites in the industry. This is still a popular subject amongst scientists.

1.3. Manufacturing Processes

Although there exists a variety of different manufacturing processes for thermoset composites, only a few of these are suitable for thick-sectioned composites manufacturing. Autoclave and Hot Press processes will be summarized in this section.

1.3.1. Autoclave (Vacuum Bagging) Process

In the past, most of thick-sectioned composites were manufactured by the autoclave molding process. The process uses pre-impregnated composite tapes (prepregs), and very complicated shapes with high fiber volume fractions can be obtained with this method.

Although the resin forms the matrix that holds the fibers together and provides stress distribution, the strength of the part is compromised if resin volume fraction is higher than necessary.

Figure 1.7 shows the proper lay-up for the autoclave process. A release film should be placed on top of the prepregs for easy disassembling after the part is fully cured. The release film also helps entrapped air, excess resin, and volatiles to escape. On top of that, a bleeder is applied in order to absorb moisture and excess resin. Subsequently, a barrier and a breather layer should be applied. The breather is a porous fabric just like the bleeder, and it creates even pressure to the part while allowing air and volatiles to escape. Finally, a vacuum bag is sealed all around the part [1]. The vacuum bag isolates the vacuum inside from the pressure in the autoclave. The vacuum applied from the vacuum nozzle allows entrapped air to escape, while the pressure in the autoclave provides proper consolidation.

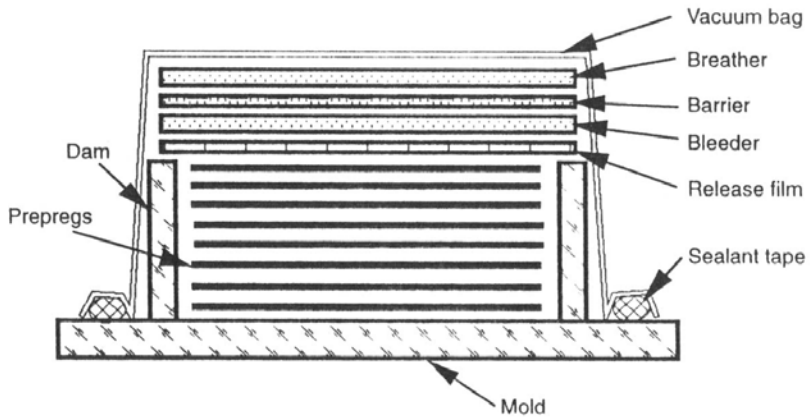

Figure 1.7. Schematic of the autoclave molding process [1]

Although the autoclave process is extremely labor intensive (each prepreg layer – which is generally 0.125 mm thick - is stacked separately, and neatly), it is an ideal process for building small quantities or prototype parts. Unfortunately, an autoclave could not be obtained during this study, thus another process, namely hot press process was used.

1.3.2. Compression Molding (Hot Press) Process

This is a plain process used for making simple parts like flat laminates. It hasn't gained much commercial use, but is suitable for laboratory scale production of simple parts

[1]. A mold is placed between two heating plates, and pressure is applied by an actuator (Figure 1.8). It is important that a release film is applied over the molds to ensure proper removal of the part after the process. It is also desirable that the tooling material and the composite has similar coefficients of thermal expansion to avoid residual stress generation.

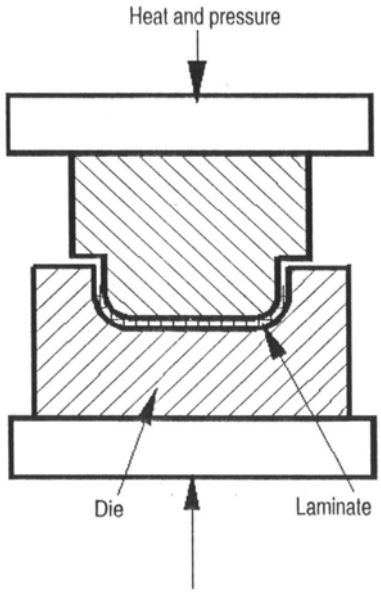

Figure 1.8. Schematic of the hot press technique [1]

2. MATHEMATICAL MODELING

A process simulation is as accurate as the mathematical model which represents the real process. However, in most situations, developing an exact model for the whole process is infeasible. Instead, as engineers, we make some assumptions and simplifications while modeling real life processes. In this chapter, such a mathematical model shall be developed for the curing process of thick-sectioned thermoset composite parts.

2.1. Thermochemical Model

The thermochemical model yields the temperature and cure distribution throughout the part. It is composed of two sub-models: Heat transfer model, and resin cure kinetics model. These models will be investigated separately.

2.1.1. Heat Transfer Model

The curing process of thermoset composite laminates can be considered as a one-dimensional, unsteady heat conduction problem with internal heat generation. The one-dimensional approximation is sufficiently accurate for flat plates or thin walled cylinders as the heat transfer in the other directions is negligible. Assuming that the convective heat transfer effect by the resin flow is also negligible and the resin and fiber are at the same temperature at any specific time, the one-dimensional model can be expressed using the conservation of energy [9]:

$$\frac{\partial}{\partial z}\left(k\frac{\partial T}{\partial z}\right)+\dot{q}=\frac{\partial}{\partial t}\left(\rho_c C_p T\right) \tag{2.1}$$

where z is the through the thickness direction, k is the anisotropic thermal conductivity, T is the temperature, $\dot{q}$ is the heat generation rate per volume (kW/m^3), t is the time, ρ_c is the composite density, and C_p is the composite specific heat.

If the composite density is considered as constant throughout the process, then the equation takes the form:

$$\frac{\partial}{\partial z}\left(k\frac{\partial T}{\partial z}\right)+\dot{q}=\rho_c\frac{\partial}{\partial t}(C_pT) \tag{2.2}$$

Since k is independent from z,

$$k\left(\frac{\partial^2 T}{\partial z^2}\right)+\dot{q}=\rho_c\frac{\partial}{\partial t}(C_pT) \tag{2.3}$$

Equation 2.3 is the governing equation of the heat transfer sub-model.

2.1.2. Resin Cure Kinetics Model

The need for a cure kinetic model arises from the dependence of the heat generation term $\dot{q}$ in the heat transfer equation to temperature and degree of cure. This interdependent nature of the process results in a coupled problem. The heat released from the exothermic curing reaction is a function of the rate of change in the polymer cure, $d\alpha/dt$ [28]:

$$\dot{q}=V_r\rho_r H_R\frac{d\alpha}{dt} \tag{2.4}$$

where V_r is the resin volume fraction, ρ_r is the resin density, H_R is the total heat of reaction, and α is the degree of cure.

As the name implies, the degree of cure α indicates the extent to which curing of a thermosetting resin has progressed, and increases from 0 to 1 as the curing reaction progresses. It is quantified by the ratio of the total heat released to the total heat of reaction H_R [28]:

$$\alpha=\frac{1}{H_R}\int_0^t\left(\frac{dq}{dt}\right)dt \tag{2.5}$$

where q is the heat generation term (kJ/kg).

It is possible to measure the value of α by using differential scanning calorimetry (DSC). However, this is not a feasible solution for industrial applications. A mathematical representation of the rate of change in the degree of cure α is crucial. The various models developed thus far can be divided into two main categories: phenomenological models and mechanistic models. Mechanistic models are derived from the stoichiometric balances of chemical species involved in the chemical reactions and require a comprehensive understanding of each elementary reaction that occurs during the process [28]. Such models are not practical due to the complex nature of the curing reaction, and various chemicals constituting the resin system. Thus, phenomenological models are more suitable for cure kinetics modeling. Phenomenological models are semi-empirical models which do not require a clean description of the chemistry involved throughout the curing process. Johnston et al. [13] presented a review of cure kinetics equations used in the literature:

Table 2.1. Cure kinetics equations [13]

Equation	Constants	Reference
$\dot{H} = \frac{d\alpha}{dt} H_R$ (2.6)	H_R = 474 kJ/kg (Hercules 3501-6)	Loos and Springer [9]
$\frac{d\alpha}{dt} = (K_1 + K_2\alpha^m)(1-\alpha)^n$ (2.7) $K_i = A_i exp(-E_i/RT)$	A_1 = 26.9 x 10^3 (s^{-1}) A_2 = 26.9 x 10^3 (s^{-1}) ΔE_1 = 57.4 kJ/mole ΔE_2 = 50.4 kJ/mole m = 0.77 n = 1.23 (Shell Epon 828)	Scott [29] – method a.
$\frac{d\alpha}{dt} = K_1(1-\alpha)^n$ (2.8) $K_i = A_i exp(-E_i/RT)$	A = 10.85 x 10^6 (s^{-1}) ΔE = 56.1 kJ/mole n = -1.0[27] (Shell Epon 828) A = 2.42 x 10^5 (s^{-1}) ΔE = 74.4 kJ/mole n = 0.78 (Ciba Geigy 6376)	Scott [29] – method a. Kenny et al. [30]
$\frac{d\alpha}{dt} = K_1(1-\alpha)^l + K_2\alpha^m(1-\alpha)^n$ (2.9) $K_i = A_i exp(-E_i/RT)$	A_1 = 3.86 x 10^6 mole/(l min) A_2 = 7.38 x 10^6 mole/(l min) ΔE_1 = 16.76 kcal/mol ΔE_2 = 15.81 kJ/mol l = 2.0 m = 0.94 n = 1.06 (TGDDM/DDS)	Lee et al. [31] – at 190 ºC

In this study, the cure kinetics model proposed by Cole et al. [32] which takes into account a shift from kinetics to diffusion control will be used:

$$\frac{d\alpha}{dt} = \frac{K\alpha^m(1-\alpha)^n}{1+e^{C(\alpha-\alpha_C)}} \tag{2.10}$$

$$\alpha_C = \alpha_{C0} + \alpha_{CT}T$$

$$K = Ae^{(-\Delta E/RT)}$$

The denominator of the expression takes into account the deceleration of the reaction as α approaches a critical degree of cure α_C, where, α_{C0} is the critical degree of cure at T = 0 K, and α_{CT} is the constant accounting for the increase in α_C with temperature. [33]

The constants in the kinetic model for AS4/8552 carbon/epoxy prepreg are taken from Ersoy et al. [33]. The constants were calculated by using the data obtained from dynamic and isothermal DSC tests.

Table 2.2. Cure kinetics constants [33]

Constant	Value	Unit	Comments
$\boldsymbol{H_R}$	574000	J/kg	Total heat of reaction
$\boldsymbol{E_a}$	65000	J/gmol	Activation energy
$\boldsymbol{A}$	$7.00\text{x}10^4$	s^{-1}	Cure rate coefficient
$\boldsymbol{m}$	0.5		First exponential constant
$\boldsymbol{n}$	1.5		Second exponential constant
$\boldsymbol{R}$	8.314	J/mol/K	Universal gas constant
$\boldsymbol{C}$	30		Diffusion constant
$\boldsymbol{\alpha_{CT}}$	$5.171\text{x}10^{-3}$	K^{-1}	Constant accounting for increase in α_C with temperature
$\boldsymbol{\alpha_{C0}}$	-1.5148		Critical degree of cure at T = 0 K

Note that these values are only valid above 20 ºC. Below that temperature, $\alpha_C = \alpha_{C0} + \alpha_{CT}T$ yields negative results, which does not make sense since degree of cure cannot be negative [28].

2.2. Material Properties

Aside from the constants in the resin cure kinetics model, the thermophysical properties of the composite material are also crucial to define the whole curing process. The thermophysical properties required for the heat transfer model include: thermal

conductivity in the transverse direction (k_t), mass density (ρ_c), and specific heat capacity (C_p). These properties are generally defined as linear functions of temperature for non-composite materials, and as linear functions of both temperature and degree of cure for thermosets and composites.

2.2.1. Thermal Conductivity

The thermal conductivity of composite materials are not necessarily the same in every direction. For example, for a unidirectional carbon/epoxy composite, thermal conductivity in the longitudinal direction is much higher than the transverse direction, since heat is transferred more rapidly along the fibers. Anyway, since a one-dimensional analysis will be carried out in this work, the only required thermal conductivity is that of the transverse direction.

Another important point is that the thermal conductivity of thermoset composite materials not only changes with temperature, but also with degree of cure. In other words, thermal conductivity is a function of both temperature and degree of cure.

$$k = f(T, \alpha)$$

There are several models developed for the prediction of transverse thermal conductivity of composite materials. One of the most popular of these models is the one developed by Springer and Tsai in 1967 [34]. In their paper, Springer and Tsai use the analogy between the response of a unidirectional composite to longitudinal shear loading and to transverse heat transfer. In the analysis it is assumed that a) the composite material is macroscopically homogenous, b) both the matrix and the fiber are locally homogenous and isotropic, c) the thermal contact resistance is negligible, d) the problem is two-dimensional, and e) the fibers are arranged in a rectangular array. The Springer-Tsai conductivity equation is [34]:

$$\frac{k_t}{k_r} = \left(1 - 2\sqrt{\frac{V_f}{\pi}}\right) + \frac{1}{B}\left(\pi - \frac{4}{\sqrt{1-\left(\frac{B^2 V_f}{\pi}\right)}}\tan^{-1}\frac{\sqrt{1-\left(\frac{B^2 V_f}{\pi}\right)}}{1+\left(\frac{B^2 V_f}{\pi}\right)}\right) \quad (2.11)$$

$$B \equiv 2\left(\frac{k_r}{k_f} - 1\right)$$

In the equation, the transverse thermal conductivity is defined in terms of the thermal conductivity of the fiber (k_f), the thermal conductivity of the resin (k_r), and the fiber volume fraction (V_f). These properties have to be identified. Johnston conducted a thorough research on material characterization [28]. The equations presented in his work are as follows [28]:

$$k_r = 0.148\ \frac{W}{mK} + \ 3.43x10^{-4}\ \frac{W}{mK℃} * T\ (℃) + \ 6.07x10^{-2}\ \frac{W}{mK} * \ \alpha \quad (2.12)$$

$$k_{ft} = 2.40\ \frac{W}{mK} + \ 5.07x10^{-3}\ \frac{W}{mK℃} * T\ (℃) \quad (2.13)$$

2.2.2. Mass Density

Although composite density changes slightly with degree of cure and temperature, it has been considered as a constant in this study for the sake of simplicity. Composite density can be easily calculated by the simple rule of mixtures:

$$\rho_c = V_f\rho_f + (1 - V_f)\rho_r \quad (2.14)$$

For the AS4/8552 material used in the experiments, these values are given as [28]:

$$\rho_f = 1790\ kg/m^3 \quad @\ T = 20\ ℃ \quad (2.15)$$

$$\rho_r = 1300\ kg/m^3 \quad @\ T = 20\ ℃,\ \alpha = 1.0$$

$$V_f = 0.573$$

2.2.3. Specific Heat Capacity

The following equation has been used for calculating the composite specific heat capacity C_p [28]:

$$C_p = \left(V_f \rho_f C_f + \left(1 - V_f\right)\rho_r C_r\right)/\left(V_f \rho_f + \left(1 - V_f\right)\rho_r\right) \quad @\ T = 20\ ^{\circ}C \qquad (2.15)$$

For the AS4/8552 material used in the experiments, these values are given as [28]:

$$C_f = 904 + (T - 75) * 2.05/^{\circ}C \quad \text{(J/kgK)} \qquad (2.16)$$

$$C_r = 1005 + (T - 20) * 3.74/^{\circ}C \quad \text{(J/kgK)}$$

T is in ℃.

3. FINITE DIFFERENCE FORMULATION

Finite difference method is a common numerical technique used for the approximate solution of partial differential equations. It is widely used in the solution of heat conduction problems. In this method, the domain is divided into a finite number of discrete intervals (Figure 3.1). Then, the derivatives in the governing equation are approximated by using one of the finite difference approximations. A relation between the nodal values is obtained with the substitution of the approximated derivative terms into the governing equation. Finally, using the knowledge of initial and boundary conditions, the nodal values are calculated at each time interval.

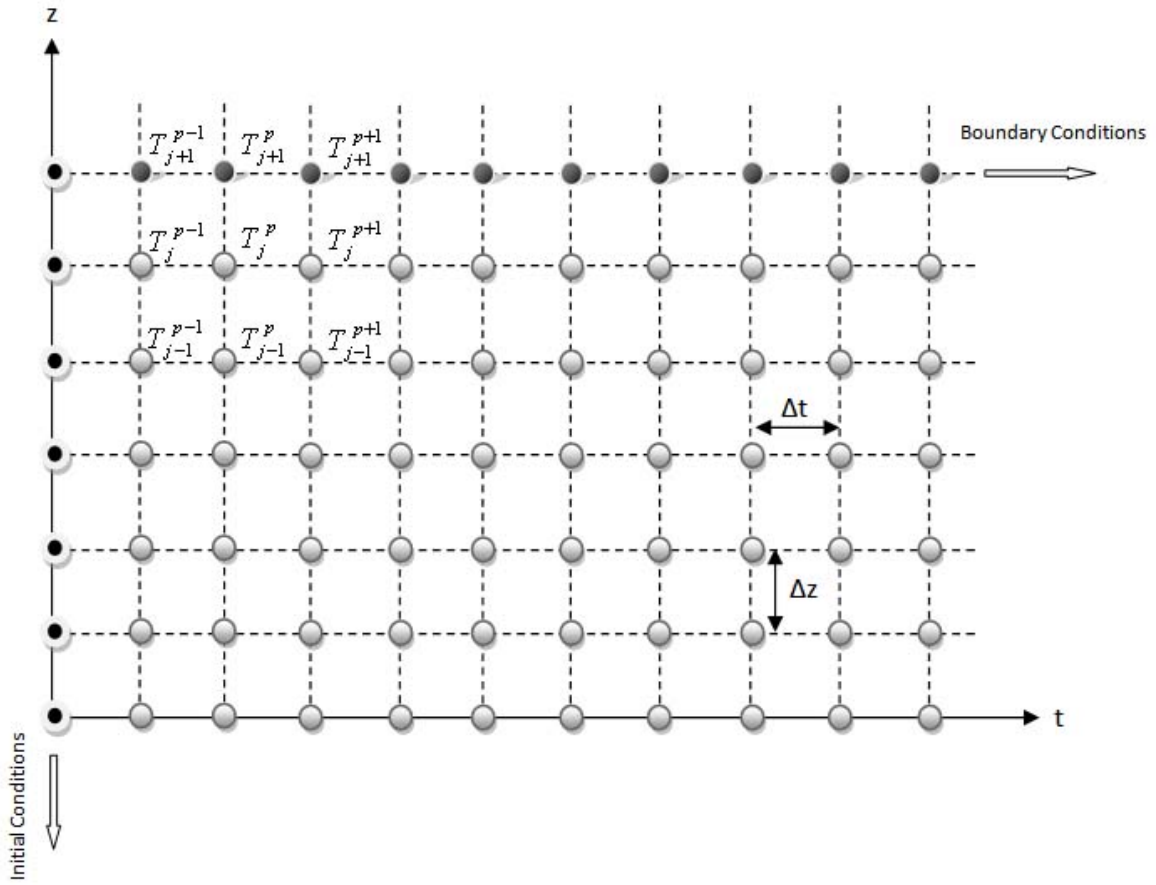

Figure 3.1. Finite difference meshing
(the subscripts denote space, and the superscripts denote time)

3.1. Finite Difference Approximations

There are various finite difference methods, which depends on different approximations of the derivatives. For example, the partial derivative $\partial T/\partial t$ may be approximated using one of the following difference methods.

3.1.1. Forward Difference

The forward difference is a finite difference defined by

$$T_j^{p+1} - T_j^p \tag{3.1}$$

Dividing this difference by the time increment yields the numerical approximation of the time derivative:

$$\frac{\partial T}{\partial t} = \frac{T_j^{p+1} - T_j^p}{\Delta t} \tag{3.2}$$

3.1.2. Backward Difference

Similarly, the time derivative using backward difference is:

$$\frac{\partial T}{\partial t} = \frac{T_j^{p} - T_j^{p-1}}{\Delta t} \tag{3.3}$$

3.1.3. Central Difference

Central difference is the mean of forward and backward differences:

$$\frac{\partial T}{\partial t} = \frac{T_j^{p+1} - T_j^{p-1}}{2\Delta t} \tag{3.4}$$

3.2. Finite Difference Methods

The solution of the finite difference equations varies according to the chosen method. While some methods can be explicitly solved by simple iterations, other implicit methods require the solution of a series of equations with n number of unknowns. Each method has some advantages over the other, which will be investigated in this section.

3.2.1. Explicit Methods

Explicit methods are the easiest and most straightforward of the two methods. The solution depends only on previous values (which are known), and can easily be solved by simple arithmetic operations. The stencil for the Forward-Time Centered-Space (FTCS) method (which is an explicit method) can be seen in Figure 3.2.

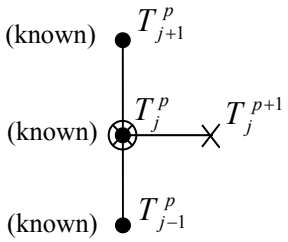

Figure 3.2. Stencil for the FTCS method [35]

For the unsteady one-dimensional parabolic diffusion equation,

$$\frac{\partial T}{\partial t} = \alpha \frac{\partial^2 T}{\partial x^2} \tag{3.5}$$

the Finite Difference Equation (FDE) using FTCS method is:

$$T_j^{p+1} = T_j^p + d\left(T_{j+1}^p - 2T_j^p + T_{j-1}^p\right) \tag{3.6}$$

At the very beginning, temperature distribution for the second time step can easily be calculated from the initial values. Using these new values, the temperature distribution for the next time step can be calculated, and so on.

3.2.2. Implicit Methods

They are called “implicit methods” because the solution at each point is implicitly specified in terms of the unknown solutions at neighboring points. In other words, the solution at every point depends on the solution at all the other points. Thus, a system of FDEs must be solved simultaneously in order to obtain the solution. [35]

It is obvious that implicit methods require more sophisticated programming and excessive computer times when compared to explicit methods. But implicit methods have a great advantage over explicit methods which may make the extra effort worthy: Most implicit methods are unconditionally stable. There are no limits on the minimum time step required to obtain a stable solution. For an implicit method, accuracy is the only consideration. On the other hand, explicit methods must satisfy a stability criterion [35]. For example, in [36], Parthasarathy has defined the following inequality for stability:

$$\frac{\bar{\alpha}\Delta t}{(\Delta z)^2} \leq 0.5 \tag{3.7}$$

This inequality can be interpreted as follows: If Δz is decreased 10 times in order to have a finer mesh, Δt has to be decreased 100 times for stability consideration. This exponential decrease in time step eventually leads to too many equations that either increase computation times beyond acceptable limits, or exceed the computer’s processing capacity. As previously discussed, most implicit methods do not have such limitations. For this reason, an implicit method, namely The Backward-Time Centered-Space (BTCS) method will be used in this study.

3.3. Application of BTCS Method to the Problem

The stencil for the BTCS method is represented in Figure 3.2. By substituting the derivative approximations into the governing equation, a series of equations should be obtained.

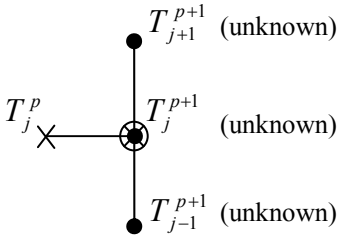

Figure 3.3. Stencil for the BTCS method [35]

The forward difference approximation of the time derivative was defined in Equation 3.2. Similarly, derivative of temperature with respect to transverse direction is:

$$\frac{\partial T}{\partial z} = \frac{T_{j+1}^{p+1} - T_j^{p+1}}{\Delta z} \tag{3.8}$$

If a consequent backward difference is applied to Equation 3.8,

$$\frac{\partial}{\partial z}\left(\frac{\partial T}{\partial z}\right) = \frac{\partial}{\partial z}\left(\frac{T_{j+1}^{p+1} - T_j^{p+1}}{\Delta z}\right) \tag{3.9}$$

$$\frac{\partial^2 T}{\partial z^2} = \frac{T_{j+1}^{p+1} - T_j^{p+1}}{\Delta z^2} - \frac{T_j^{p+1} - T_{j-1}^{p+1}}{\Delta z^2} \tag{3.10}$$

the second derivative of temperature with respect to transverse direction can be approximated as:

$$\frac{\partial^2 T}{\partial z^2} \cong \frac{T_{j+1}^{p+1} - 2T_j^{p+1} + T_{j-1}^{p+1}}{\Delta z^2} \tag{3.11}$$

Finally, the time derivative of the heat capacity has to be defined. However, heat capacity depends on temperature, and if its derivative were defined as:

$$\frac{\partial C}{\partial t} = \frac{C_j^{p+1} - C_j^p}{\Delta t} \tag{3.12}$$

then one more unknown term (C_j^{p+1}) would appear in each equation. Instead, "lagging" will be used by defining the time derivative of the heat capacity as:

$$\frac{\partial C}{\partial t} = \frac{C_j^p - C_j^{p-1}}{\Delta t} \tag{3.13}$$

Since the time index of C_j^{p-1} will be zero for time step 1, a separate sequence has to be carried out for the first iteration.

Introducing (3.10) and (3.13) into (2.3)

$$k\left(\frac{T_{j+1}^{p+1} - 2T_j^{p+1} + T_{j-1}^{p+1}}{\Delta z^2}\right) + \dot{q} = \rho\left[T\left(\frac{C_j^p - C_j^{p-1}}{\Delta t}\right) + C\left(\frac{T_j^{p+1} - T_j^p}{\Delta t}\right)\right] \tag{3.14}$$

Before going any further, it is important to emphasize one point. As previously mentioned, the thermochemical model adopted in this study is composed of two sub-models. Namely, the heat transfer model which predicts the temperature distribution throughout the part, and the resin cure kinetics model which predicts the degree of cure distribution. Actually, these two sub-models are coupled. This suggests that the resin reaction and heat generation rates vary continuously with time. However, the sub-models are treated as uncoupled in this study. In other words, they are assumed to remain constant during each time step. This simplifying assumption is accurate if sufficiently small time steps are chosen.

The nodal values of T, C, k, and $\dot{q}$ in Equation 3.13 should also be assigned according to the current time step. Replacing them with

$$T = T_j^p$$
$$C = C_j^p$$
$$k = k_j^p$$
$$\dot{q} = \dot{q}_j^p$$

yields:

$$\frac{k_j^p}{(\Delta z)^2}\left(\boldsymbol{T_{j+1}^{p+1}} - 2\boldsymbol{T_j^{p+1}} + \boldsymbol{T_{j-1}^{p+1}}\right) + \dot{q}_j^p = \frac{\rho}{\Delta t}\left[T_j^p\left(C_j^p - C_j^{p-1}\right) + C_j^p\left(\boldsymbol{T_j^{p+1}} - T_j^p\right)\right] \tag{3.15}$$

Unknown values are written in bold letters for convenience.

Defining thermal diffusivity $\overline{\alpha}$, and d for simplicity:

$$\overline{\alpha} = \frac{k}{\rho C} \tag{3.16}$$

$$d = \frac{\overline{\alpha}\Delta t}{(\Delta z)^2}$$

Equation 3.15 simplifies as:

$$\frac{\Delta t}{\rho C_j^p}\frac{k_j^p}{(\Delta z)^2}\left(\boldsymbol{T_{j+1}^{p+1}} - 2\boldsymbol{T_j^{p+1}} + \boldsymbol{T_{j-1}^{p+1}}\right) + \dot{q}_j^p\frac{\Delta t}{\rho C_j^p} = \left[T_j^p\left(1 - \frac{C_j^{p-1}}{C_j^p}\right) + \boldsymbol{T_j^{p+1}} - T_j^p\right] \tag{3.17}$$

$$d_j^p\left(\boldsymbol{T_{j+1}^{p+1}} - 2\boldsymbol{T_j^{p+1}} + \boldsymbol{T_{j-1}^{p+1}}\right) + \frac{\dot{q}_j^p\Delta t}{\rho C_j^p} = \boldsymbol{T_j^{p+1}} - \frac{C_j^{p-1}}{C_j^p}T_j^p \tag{3.18}$$

$$\frac{C_j^{p-1}}{C_j^p}T_j^p + \frac{\dot{q}_j^p\Delta t}{\rho C_j^p} = \left(1 + 2d_j^p\right)\boldsymbol{T_j^{p+1}} - d_j^p\left(\boldsymbol{T_{j+1}^{p+1}} + \boldsymbol{T_{j-1}^{p+1}}\right) \tag{3.19}$$

Equation 3.19 represents the relation between the nodes. If n is the number of space steps and m is the number of time steps, then n x m number of such equations may be written and solved for n x m number of unknowns. Fortunately, these equations do not necessarily have to be solved all at once. The solution will be discussed in Section 3.5.

3.4. Boundary Conditions

The correct specification of the boundary conditions is vital for an accurate simulation of the process. Even if a perfect model which exactly represents the process is used, a bad judgment in the determination of boundary conditions would lead to misleading results. The most frequently encountered boundary conditions in heat transfer problems are [37]:

1. Prescribed temperature
2. Prescribed heat flux
3. No heat flux (insulation or symmetry)

4. Heat transfer to the ambient by convection
5. Heat transfer to the ambient by radiation

In the experimental setup used in this study, the thermocouples are placed as close to the mold surface as possible (Figure 3.4). The temperatures at the center of the molds are measured by two K-type thermocouples, and two Proportional-Integral-Derivative (PID) controllers effectively control the temperature at these points, according to the cure cycle. Thus, both boundaries may be specified as "prescribed temperature" boundaries. The problem may be solved with these two boundary conditions. However, by taking advantage of the symmetry of the part, it is possible to model only one half of the part, and consequently halve the computational effort.

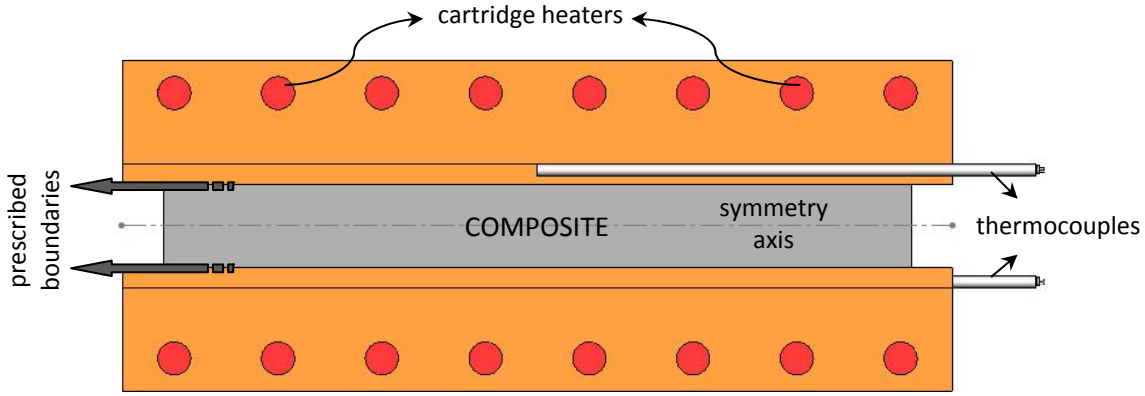

Figure 3.4. Representation of the heating setup

In Figure 3.5 the application of the boundary conditions to the finite difference mesh is represented. The prescribed boundary condition is defined as:

$$T_1^p = T_{curing}$$

where T_{curing} is the vector containing the temperature profile of the cure cycle.

Since the part is symmetrical, the other boundary may be defined as (see Figure 3.5):

$$T_{n+1}^p = T_{n-1}^p$$

The knowledge of the boundary conditions are necessary but not sufficient for the solution of the equations. The initial conditions also have to be defined. It is assumed that at the beginning the part has a uniform temperature that is equal to the ambient temperature. This assumption is accurate if sufficient time has passed after the prepreg layers are taken out of the refrigerator.

$$T_j^1 = T_{amb}$$

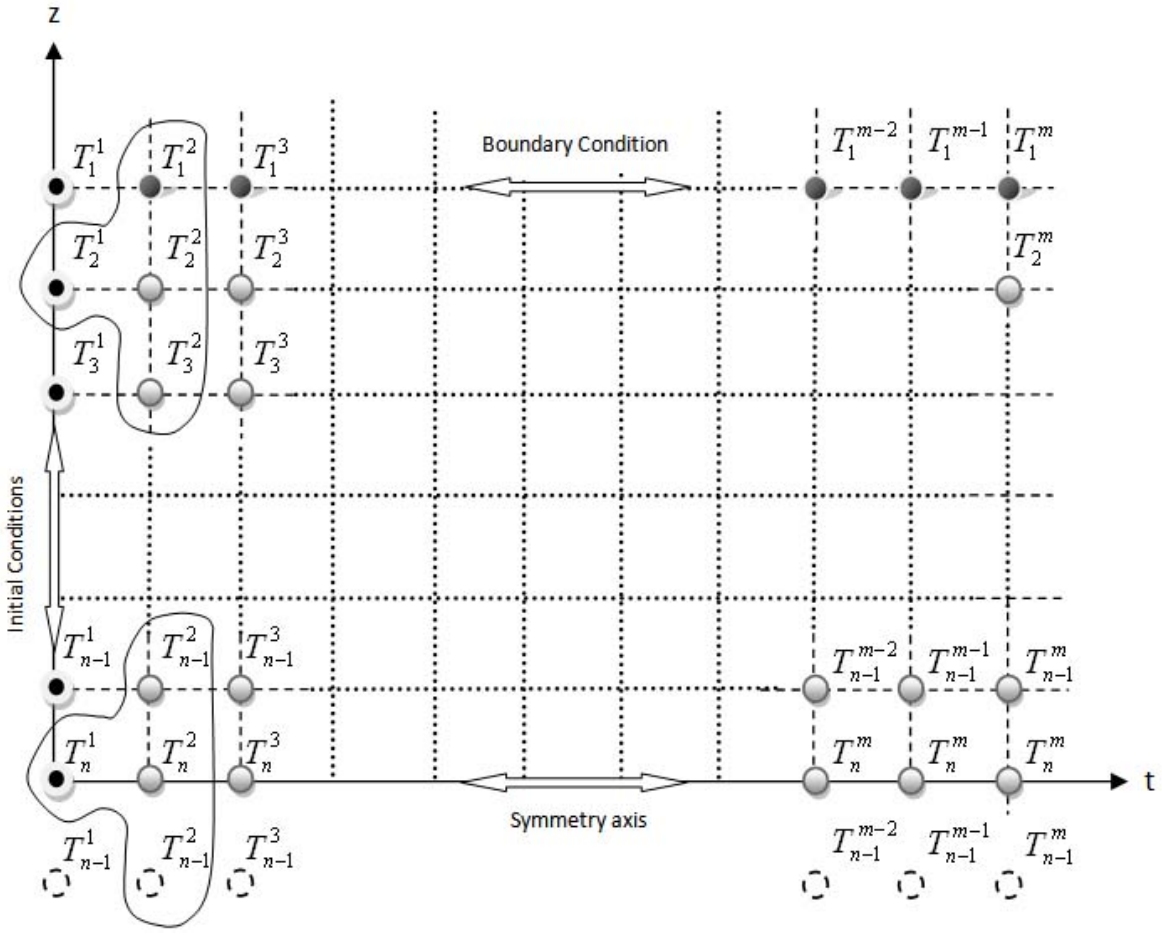

Figure 3.5. Finite difference mesh for half of the part

3.5. Solution of the Equations

Let us make a simple calculation to estimate the extent of the problem we are dealing with. Let us roughly assume that the process lasts 4 hours, and that we are manufacturing a 20 mm thick composite plate. If we set the time step to 10 seconds and space step to 0.1

mm, we would have 1440 discrete time intervals and 100 space intervals (the part is symmetric, therefore we analyze only one half). This amounts 144000 equations with 144000 unknowns. We have to find a systematic way to solve these equations. Representing the equations in matrix form is the first step.

At p = 1 (initial time), the equations are as follows:

$$\frac{C_2^0}{C_2^1}T_2^1 + \frac{\dot{q}_2^1 \Delta t}{\rho C_2^1} = (1 + 2d_2^1)\boldsymbol{T_2^2} - d_2^1\left(\boldsymbol{T_3^2} + \boldsymbol{T_1^2}\right) \tag{3.20}$$

$$\frac{C_3^0}{C_3^1}T_3^1 + \frac{\dot{q}_3^1 \Delta t}{\rho C_3^1} = (1 + 2d_3^1)\boldsymbol{T_3^2} - d_3^1\left(\boldsymbol{T_4^2} + \boldsymbol{T_2^2}\right)$$

$$\vdots$$

$$\frac{C_{n-1}^0}{C_{n-1}^1}T_{n-1}^1 + \frac{\dot{q}_{n-1}^1 \Delta t}{\rho C_{n-1}^1} = (1 + 2d_{n-1}^1)\boldsymbol{T_{n-1}^2} - d_{n-1}^1\left(\boldsymbol{T_n^2} + \boldsymbol{T_{n-2}^2}\right)$$

$$\frac{C_n^0}{C_n^1}T_n^1 + \frac{\dot{q}_n^1 \Delta t}{\rho C_n^1} = (1 + 2d_n^1)\boldsymbol{T_n^2} - d_n^1\left(\boldsymbol{T_{n-1}^2} + \boldsymbol{T_{n-1}^2}\right)$$

n-1 such equations can be written for p = 1. T_1^2 is already known from the boundary condition, and T_2^1, T_3^1, …, T_n^1 are known from the initial condition. So, for each time step there exists n-1 equations with n-1 unknowns (T_2^2, T_3^2, …, T_n^2). Instead of solving n x m equations with n x m unknowns all at once, each time step can be analyzed individually.

If these equations are written in the matrix form of

$$[A]\vec{T} = \vec{b} \tag{3.21}$$

they can be easily solved. Here, $[A]$ is the coefficients matrix, $\vec{T}$ is the solution vector, and $\vec{b}$ is the right hand side (RHS) vector. In matrix form, the equations take the following form:

$$\begin{bmatrix} * & * & * & * & * & * & * \\ -d_2^1 & \left(1+2d_2^1\right) & -d_2^1 & 0 & \cdots & 0 & 0 \\ 0 & -d_3^1 & \left(1+2d_3^1\right) & -d_3^1 & 0 & \cdots & 0 \\ \vdots & \ddots & \ddots & \ddots & \ddots & \ddots & \vdots \\ 0 & \cdots & 0 & -d_{n-2}^1 & \left(1+2d_{n-2}^1\right) & -d_{n-2}^1 & 0 \\ 0 & 0 & \cdots & 0 & -d_{n-1}^1 & \left(1+2d_{n-1}^1\right) & -d_1^{n-1} \\ 0 & 0 & 0 & \cdots & 0 & -2d_n^1 & \left(1+2d_n^1\right) \end{bmatrix} \begin{bmatrix} T_1^2 \\ T_2^2 \\ T_3^2 \\ \vdots \\ T_{n-2}^2 \\ T_{n-1}^2 \\ T_n^2 \end{bmatrix} = \begin{bmatrix} * \\ \frac{C_2^0}{C_2^1}T_2^1 + \frac{\dot{q}_2^1\Delta t}{\rho C_2^1} \\ \frac{C_3^0}{C_3^1}T_3^1 + \frac{\dot{q}_3^1\Delta t}{\rho C_3^1} \\ \vdots \\ \frac{C_{n-2}^0}{C_{n-1}^1}T_{n-2}^1 + \frac{\dot{q}_{n-2}^1\Delta t}{\rho C_{n-2}^1} \\ \frac{C_{n-1}^0}{C_{n-1}^1}T_{n-1}^1 + \frac{\dot{q}_{n-1}^1\Delta t}{\rho C_{n-1}^1} \\ \frac{C_n^0}{C_n^1}T_n^1 + \frac{\dot{q}_n^1\Delta t}{\rho C_n^1} \end{bmatrix} \quad (3.22)$$

From symmetry

T_1^2 is known from the boundary condition. The first row and first column have to be eliminated to avoid singularity.

$$\begin{bmatrix} * & * & * & * & * & * & * \\ -d_2^1 & \left(1+2d_2^1\right) & -d_2^1 & 0 & \cdots & 0 & 0 \\ 0 & -d_3^1 & \left(1+2d_3^1\right) & -d_3^1 & 0 & \cdots & 0 \\ \vdots & \ddots & \ddots & \ddots & \ddots & \ddots & \vdots \\ 0 & \cdots & 0 & -d_{n-2}^1 & \left(1+2d_{n-2}^1\right) & -d_{n-2}^1 & 0 \\ 0 & 0 & \cdots & 0 & -d_{n-1}^1 & \left(1+2d_{n-1}^1\right) & -d_1^{n-1} \\ 0 & 0 & 0 & \cdots & 0 & -2d_n^1 & \left(1+2d_n^1\right) \end{bmatrix} \begin{bmatrix} T_1^2 \\ T_2^2 \\ T_3^2 \\ \vdots \\ T_{n-2}^2 \\ T_{n-1}^2 \\ T_n^2 \end{bmatrix} = \begin{bmatrix} * \\ \frac{C_2^0}{C_2^1}T_2^1 + \frac{\dot{q}_2^1\Delta t}{\rho C_2^1} \\ \frac{C_3^0}{C_3^1}T_3^1 + \frac{\dot{q}_3^1\Delta t}{\rho C_3^1} \\ \vdots \\ \frac{C_{n-2}^0}{C_{n-1}^1}T_{n-2}^1 + \frac{\dot{q}_{n-2}^1\Delta t}{\rho C_{n-2}^1} \\ \frac{C_{n-1}^0}{C_{n-1}^1}T_{n-1}^1 + \frac{\dot{q}_{n-1}^1\Delta t}{\rho C_{n-1}^1} \\ \frac{C_n^0}{C_n^1}T_n^1 + \frac{\dot{q}_n^1\Delta t}{\rho C_n^1} \end{bmatrix} \quad (3.23)$$

The contribution of the eliminated terms must be added to the RHS vector.

From Boundary Condition

$$\begin{bmatrix} \left(1+2d_2^1\right) & -d_2^1 & 0 & \cdots & 0 & 0 \\ -d_3^1 & \left(1+2d_3^1\right) & -d_3^1 & 0 & \cdots & 0 \\ 0 & \ddots & \ddots & \ddots & \ddots & \vdots \\ \vdots & 0 & -d_{n-2}^1 & \left(1+2d_{n-2}^1\right) & -d_{n-2}^1 & -d_1^{n-1} \\ 0 & \cdots & 0 & -d_{n-1}^1 & \left(1+2d_{n-1}^1\right) & -d_{n-1}^1 \\ 0 & 0 & \cdots & 0 & -2d_n^1 & \left(1+2d_n^1\right) \end{bmatrix} \begin{bmatrix} T_2^2 \\ T_3^2 \\ \vdots \\ T_{n-2}^2 \\ T_{n-1}^2 \\ T_n^2 \end{bmatrix} = \begin{bmatrix} \frac{C_2^0}{C_2^1}T_2^1 + \frac{\dot{q}_2^1\Delta t}{\rho C_2^1} + d_2^1 T_1^2 \\ \frac{C_3^0}{C_3^1}T_3^1 + \frac{\dot{q}_3^1\Delta t}{\rho C_3^1} \\ \vdots \\ \frac{C_{n-2}^0}{C_{n-1}^1}T_{n-2}^1 + \frac{\dot{q}_{n-2}^1\Delta t}{\rho C_{n-2}^1} \\ \frac{C_{n-1}^0}{C_{n-1}^1}T_{n-1}^1 + \frac{\dot{q}_{n-1}^1\Delta t}{\rho C_{n-1}^1} \\ \frac{C_n^0}{C_n^1}T_n^1 + \frac{\dot{q}_n^1\Delta t}{\rho C_n^1} \end{bmatrix} \quad (3.24)$$

Multiplying both sides of Equation 3.24 by $[A]^{-1}$ yields

$$[A]^{-1}[A]\vec{T} = [A]^{-1}\vec{b} \tag{3.25}$$

$$\vec{T} = [A]^{-1}\vec{b} \tag{3.26}$$

If the coefficient matrix $[A]$ and RHS vector $\vec{b}$ are generated for each iteration, the temperature distribution can be calculated by using Equation 3.26. The computer code for this procedure will be examined next.

3.6. Computer Code for BTCS Method

Figure 3.6. shows a simplified flowchart of the algorithm for the Finite Difference Analysis (FDA). The algorithm executes two nested loops; while the first loop generates the equations for each space node within a constant time step, the second loop calculates the temperature distribution for each time step by solving a series of equations.

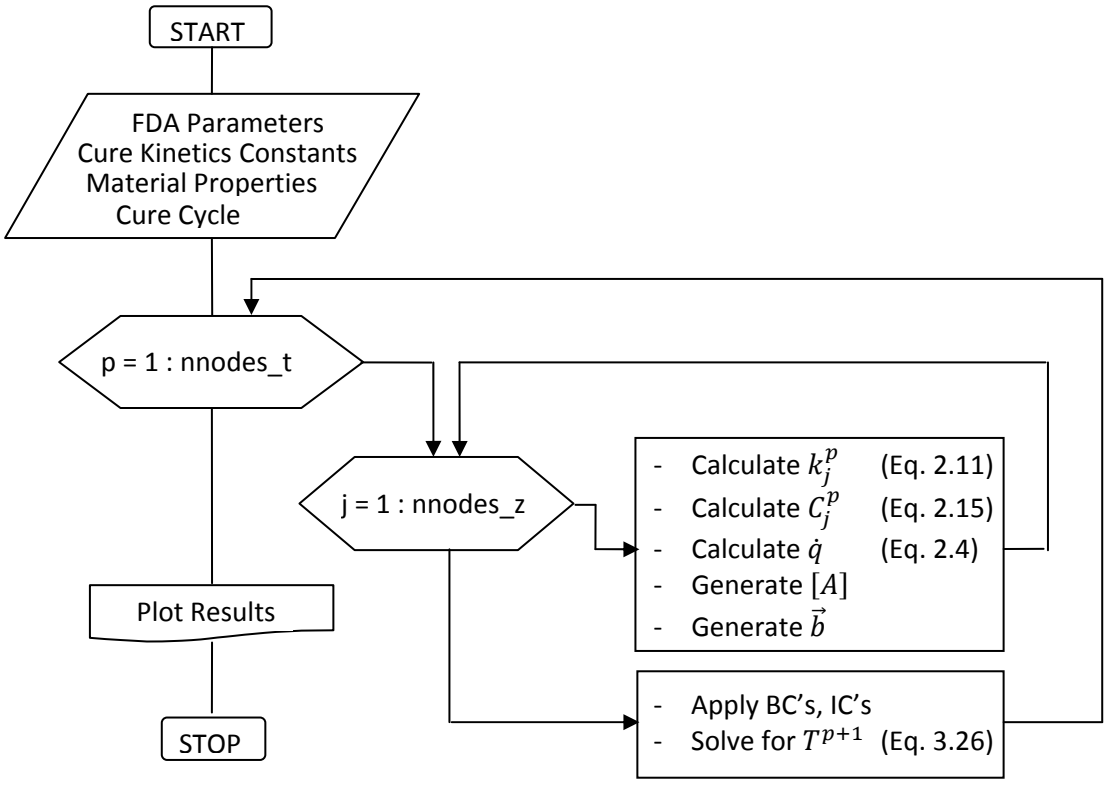

Figure 3.6. Flowchart of the FDA algorithm

4. CURE CYCLE OPTIMIZATION

It was previously discussed that the temperature gradients could be reduced by applying slower heating rates, at the expense of increased manufacturing time and cost. Vice versa, manufacturing time and cost may be reduced by increasing the heating rates. In between these two extremes, there exists an optimal temperature profile which minimizes the manufacturing time, while at the same time keeping the temperature gradients below a desired limit. Actually, there are infinite number of such potential profiles. Thus, a method to quantify the quality of these profiles, and an optimization algorithm should be selected to guide us through our search for the optimum cure cycle (OCC).

Optimization algorithms may be categorized in three distinct categories: zeroth, first, and second order methods. Zeroth order methods only depend on the function values calculated at the design points. In contrast, first and second order methods also rely on first and second derivatives of the function, respectively [38]. Since zeroth order methods do not involve any derivatives of the function, they tend to be less complex in programming. However, first and second order methods are inherently more effective, as they "know" if the function is moving in a better direction or not.

4.1. Sequential Simplex Optimization Algorithm

Due to the complexity of the equations, calculating the derivatives of the function with respect to the variables is virtually impossible. For this reason, a zeroth order method, namely "Sequential Simplex" algorithm, which was developed by Nelder and Mead in 1965 has been used in this study [39]. Sequential Simplex is a common optimization algorithm which is capable of dealing with nonlinear functions in many-dimensional space.

The algorithm begins with an N-dimensional geometrically regular shape called simplex, where N is the number of design parameters. Although the algorithm also works with other initial points, a simplex is the most efficient and time saving figure for searching

the design space [38]. Spendley et al. proposed the following equation for generating a simplex [40].

$$x_j = x_0 + p\boldsymbol{e_j} + \sum_{\substack{k=1 \\ k\neq j}}^{N} q\boldsymbol{e_k}, \qquad j = 1, \dots, N \tag{4.1}$$

$$p = a\left(\sqrt{N+1} + N - 1\right)/N\sqrt{2} \tag{4.2}$$

$$q = a\left(\sqrt{N+1} - 1\right)/N\sqrt{2} \tag{4.3}$$

where x_0 is the initial point, $\boldsymbol{e_k}$ is the unit vector along the k coordinate, and a is the size of the simplex.

Equation 4.1 yields a line segment in 1-dimension, an equilateral triangle of side a in 2-dimensions, a tetrahedron in 3-dimensions, and so on (Figure 4.1). In the following pages the algorithm is examined for the 2-dimensional case, since it is easier to visualize the operations in this dimension.

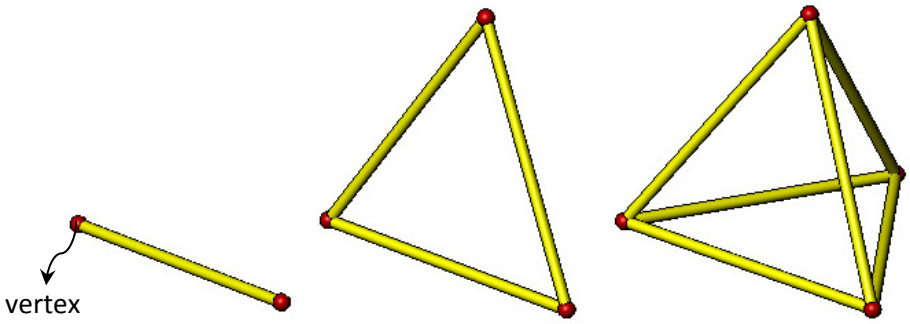

Figure 4.1. Simplex geometries for 1-D, 2-D, and 3-D, respectively

After the simplex is generated, the function is evaluated at each vertex. Subsequently, these vertices are sorted according to their function values. The vertex having the lowest (therefore best) function value f_l is denoted by x_l. Similarly, the vertex having the highest function value f_h is denoted by x_h, and the vertex with the second highest function value f_s by x_s (Figure 4.2-a). Then, a new point, namely x_r, that is the

reflection of the worst point with respect to the centroid $\bar{x}$ is calculated (Figure 4.2-b). The centroid $\bar{x}$ is the centroid of the points excluding the worst point, and defined as:

$$\bar{x} = \frac{1}{N}\sum_{i=0}^{N} x_i, \qquad i \neq h \tag{4.4}$$

The reflection point x_r is calculated by:

$$x_r = \bar{x} + (\bar{x} - x_h) \tag{4.5}$$

At the end of each iteration, the worst point is replaced by a new (and better) point, which is found by using four simple operations: *reflection*, *expansion*, *contraction*, and *shrinkage*. Figure 4.2 shows the graphical representation of these operations and Figure 4.3 shows the flowchart of the sequential simplex algorithm.

The contraction point x_c is calculated by (Figure 4.2-c):

$$x_c = \bar{x} + \frac{1}{2}(x_h - \bar{x}) \tag{4.7}$$

and the expansion point x_e is calculated by (Figure 4.2-d):

$$x_e = \bar{x} + 2(x_r - \bar{x}), \tag{4.6}$$

For the shrinkage operation, all points are replaced by a new set of points defined by (Figure 4.2-e):

$$x_i = x_i + \tfrac{1}{2}(x_l - x_i), \qquad i = 0,1,\dots,N \tag{4.8}$$

This operation halves the distance between the old points and the best point, hence the name *shrinkage*.

The action of replacing the worst set with a new and better set allows the solution to come near to an optimum point at each iteration.

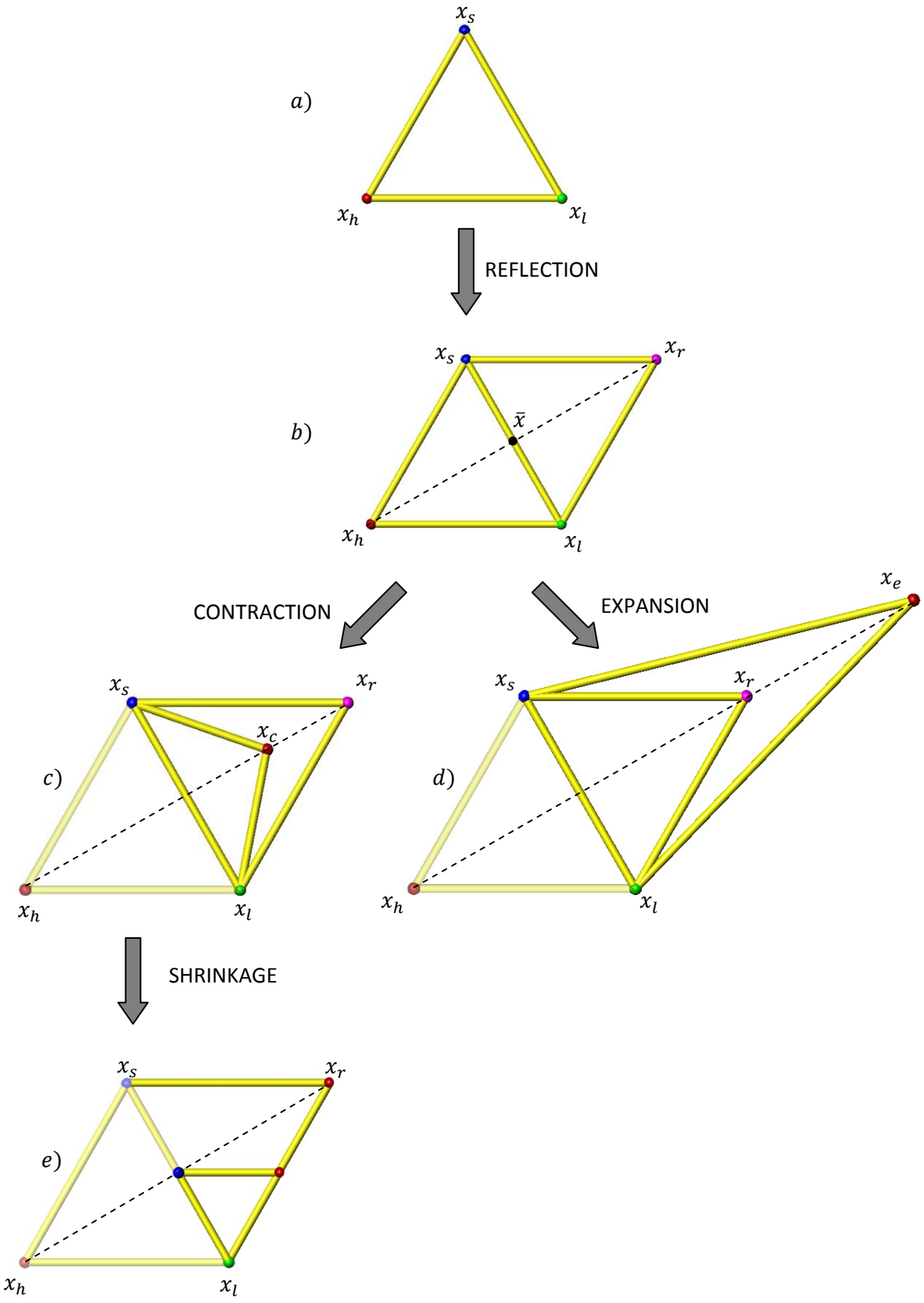

Figure 4.2. Graphical representation of the operations

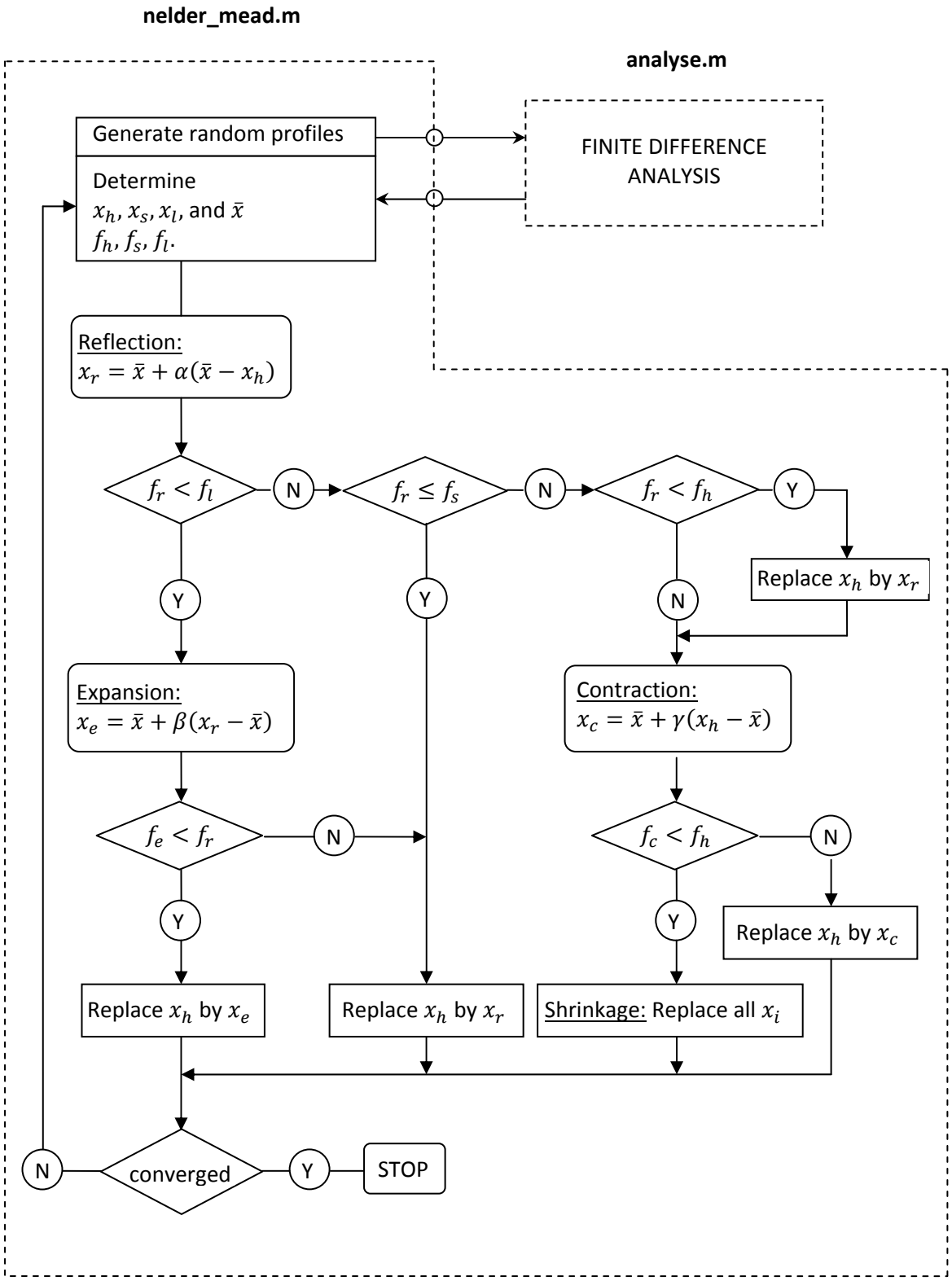

Figure 4.3. Flowchart of the Sequential Simplex algorithm

The algorithm is repeated until convergence is satisfied. For the convergence criterion, Nelder and Mead [39] suggested the following inequality:

$$\left\{\frac{1}{1+n}\sum_{i=0}^{n}[f_i - f(\bar{x})]^2\right\}^{\frac{1}{2}} < \epsilon \tag{4.9}$$

where ϵ is a sufficiently small number which meets the accuracy requirement.

The accuracy of the computer code (written in MATLAB) has been checked by running it for a well known function, namely Himmelblau's function. It is a 2-dimensional, multimodal function that has one global optimum, and 3 local optima. These properties make the function ideal for testing optimization algorithms. It is defined as:

$$f(x) = (x_1^2 + x_2 - 11)^2 + (x_1 + x_2^2 - 7)^2 \tag{4.10}$$

and its minima are:

$f\,(3,2) = 0$ → Global Minimum

$f\,(-3.78,-3.28) = 0.0054$

$f\,(-2.81,3.13) = 0.0085$ → Local Minima

$f\,(3.58,-1.85) = 0.0011$

The contour map of Himmelblau's function is shown in Figure 4.4. The peaks in dark color are the minimum points of the function. The minimum on the upper-right corner is the global minimum, and the remaining ones are the local minima.

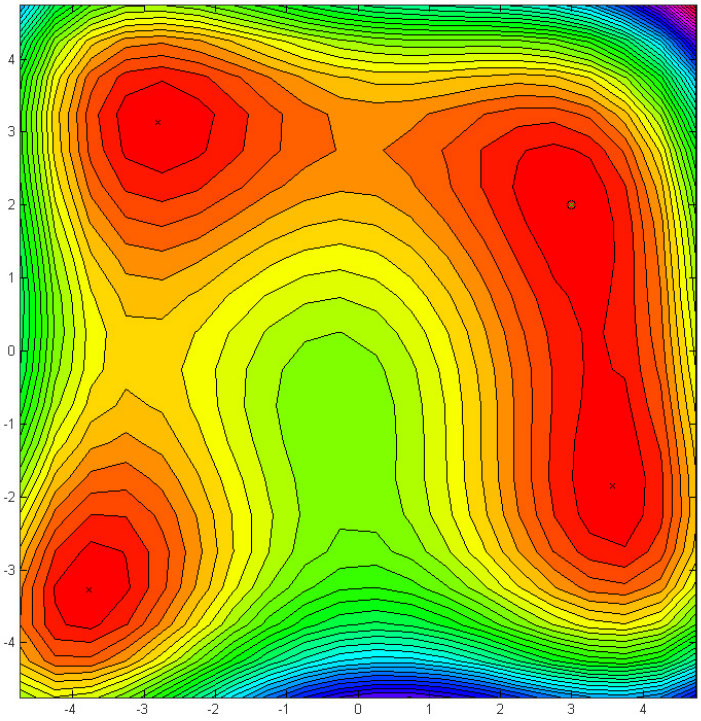

Figure 4.4. Contour map of Himmelblau's function

The sequential simplex method requires that the function is unimodal (having only one minimum) [38]. Otherwise, it is very likely that the algorithm will be stuck to a local minimum. Figure 4.5 shows different results for different base points. In the figure on the left, the algorithm converges to one of the local minima. A different base point is selected in the figure on the right, and the algorithm converges to the global minimum this time.

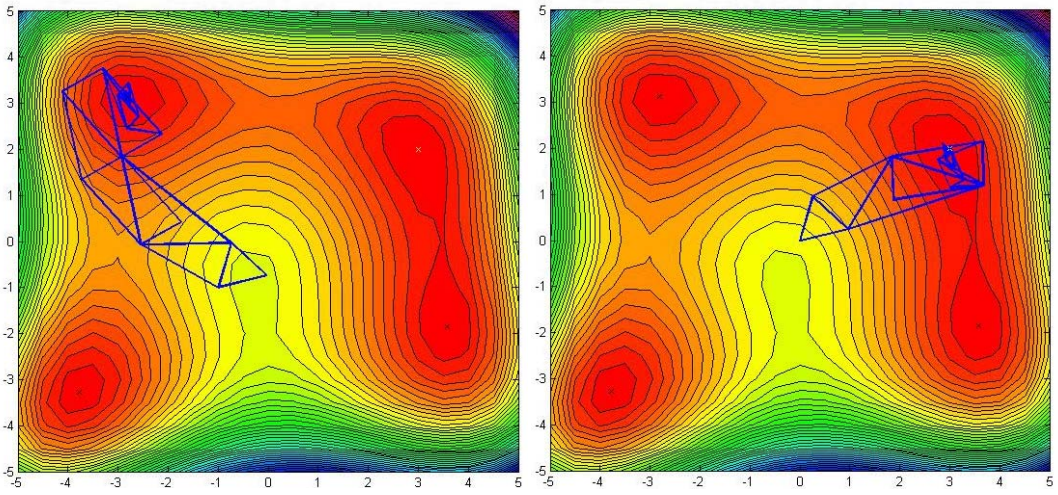

Figure 4.5. Results of different base points

However, by repeating the optimization procedure many times, starting from different points within the design space, convergence to the global minimum can be guaranteed [41].

4.2. Constraint Optimization

Most engineering problems involve some limits, or constraints on the allowable design parameters. For example, when designing a truss system, a constraint such that $\sigma_{max} < \sigma_{yield}$ may be defined. The effects of these constraints should be reflected on the optimization procedure. Although sequential simplex is an unconstraint optimization method, it is possible to convert a constraint optimization problem into an unconstraint one. One way to do that is to use an exterior penalty function method.

4.2.1. Exterior Penalty Function Method

The main idea behind the penalty function method is to replace the constraints with penalties instead of applying them separately. When using an exterior penalty function, the penalty is only applied outside the feasible domain. [38]. For example, in an optimization problem like:

minimize $f(x)$ such that $g(x) < 0$

The constraint can be eliminated by replacing the problem with:

minimize $f(x) + p * < g >^2$

where p is an appropriate penalty coefficient, and $< g >$ is the positive part of g. In this way, the constraint is included in the function itself.

4.3. Application of the Method to the Problem

An objective function, and constraints (if any) should be defined for the solution of any optimization problem. In this work, the problem was stated as: complete the process in

the shortest time possible, without compromising the part quality. Thus, the objective is to find the shortest processing time possible, in a design space limited by some constraints. These constraints involve any condition that reduces the part quality. The most important of these constraints may be defined as:

- The thermal gradients throughout the part must not exceed a pre-specified value.
- The temperature anywhere must not exceed the resin's degradation temperature.
- At the end of the process, degree of cure anywhere in the part must have reached a pre-specified value to ensure full curing.
- Residual stresses must be minimal
- Void growth inside the part must be minimal

Further constraints may also be added to the list. However, the applicability of these constraints depend on the mathematical model. For instance, adding a constraint regarding the growth of voids inside the part is not possible without a resin flow sub-model.

In addition to these constraints, other constraints representing the limits of the experimental setup may also be required. For example, if the optimal temperature profile obtained is exceeding the heating capacity of the mold, a constraint defining the maximum heating rate of the setup should be added to guarantee a feasible solution.

4.3.1. Objective Function

In this study, decreasing the temperature gradients has been the primary concern, so it is the only constraint included in the objective function. Since residual stress and resin flow sub-models have not been developed, they have not been included in the optimization procedure, either. The problem is defined as:

minimize t such that $\Delta T \leq 5\ ^{o}C$

where t is the total processing time, and ΔT is the maximum temperature gradient throughout the part. Figure 4.6 represents the calculation of the objective function using external penalty function.

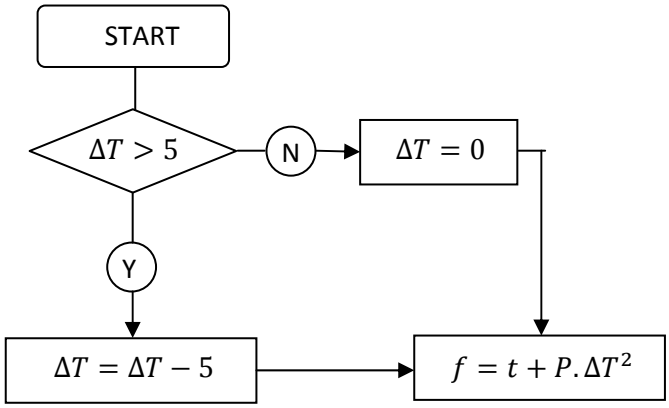

Figure 4.6. Calculation of the objective function

4.3.2. Design Parameters

Design parameters are the independent variables that are required to define the whole process. In fact, the objective function is a function of these design parameters. Hence, optimizing the process is actually finding the optimum values for each parameter.

A cure cycle is indeed a temperature profile over time. Since defining each point on this profile as design parameters is not possible, the cure cycle should be represented with discrete design points (Figure 4.7).

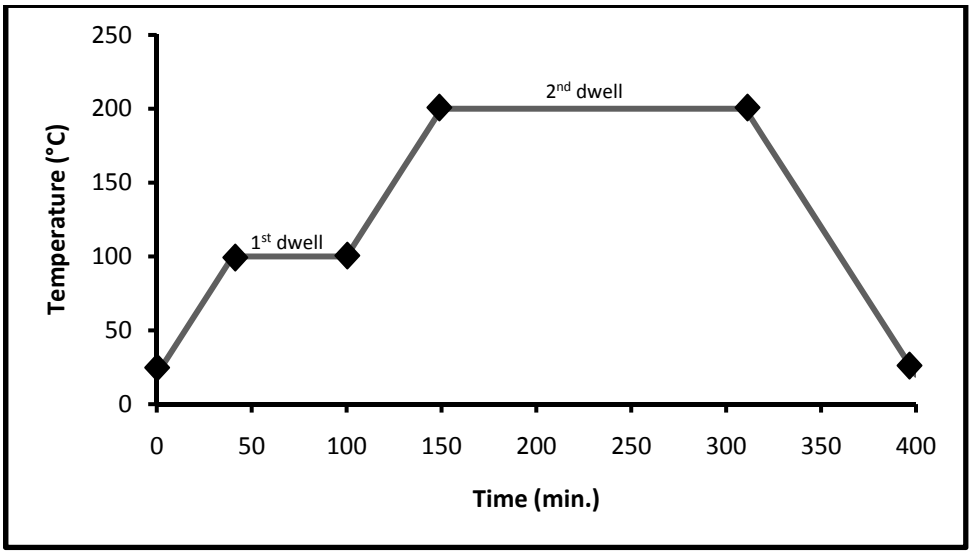

Figure 4.7. Representation of the cure cycle with discrete points

However, there is also a limit to the number of allowable design parameters. The sequential simplex optimization algorithm is proved to be inefficient for more than 10 parameters [38]. Since each point on the profile is defined by two parameters (one for temperature, and one for time), only 5 points may be used for defining the cure cycle. Anyway, by selecting a common time interval, and analyzing each phase separately, it is possible to define a wide range of profiles (Figure 4.8). For instance, for the 1st ramp in Figure 4.8, the design parameters consist of 1 common time interval and 9 temperature values. Again, the 2nd ramp may be defined by one common time interval and 9 temperature points. This approach allows the design of more complex curves.

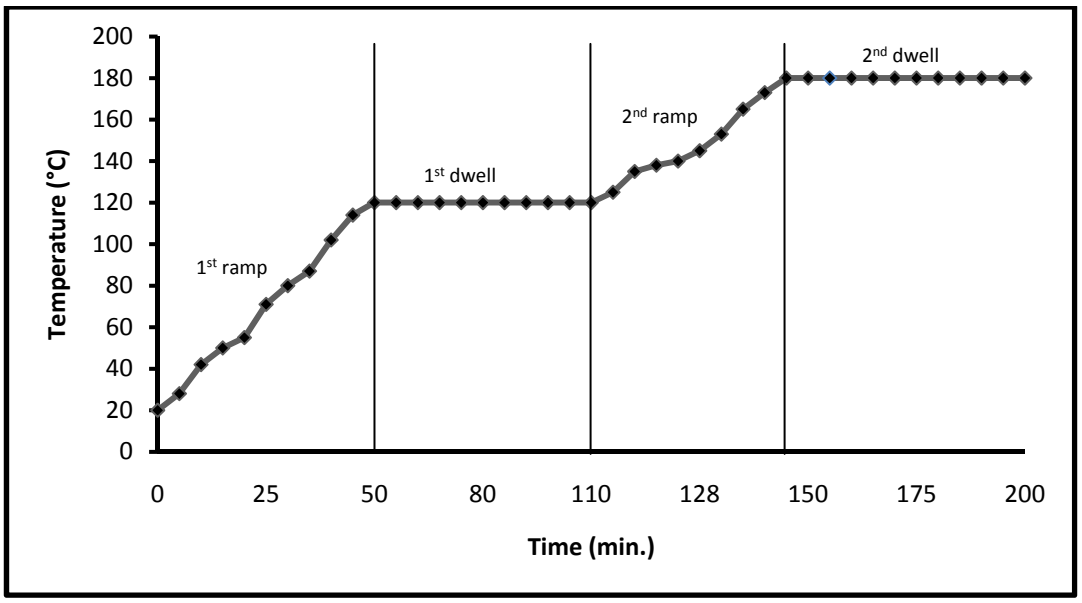

Figure 4.8. Representation of the cure cycle by a common time interval

5. EXPERIMENTAL SETUP

An experimental setup has been prepared in order to verify the results obtained from the analysis (see Figure 5.1). The setup consists of a hydraulic unit, two heating molds, a steel frame, a temperature control unit, and a data acquisition device. These elements constituting the experimental setup shall be investigated individually in this chapter.

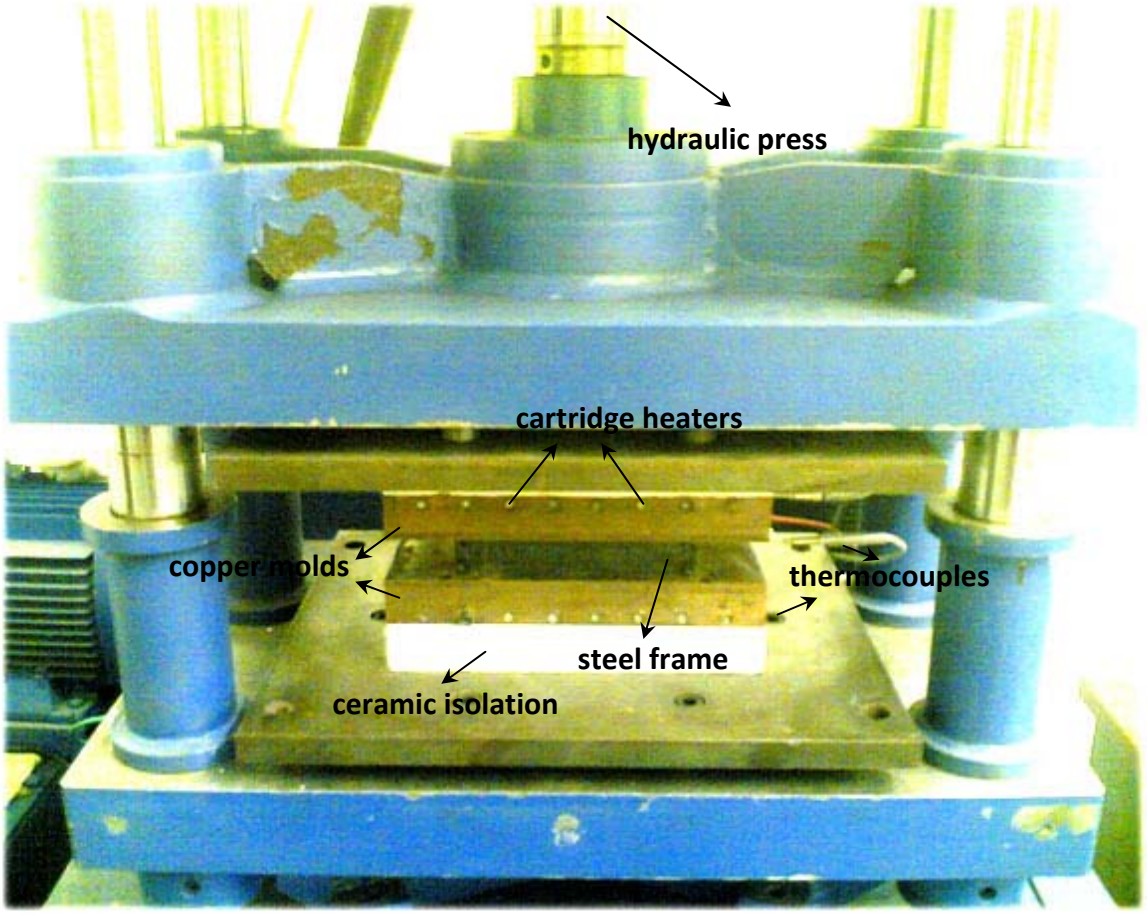

Figure 5.1. Experimental setup

5.1. Hydraulic Unit

As previously discussed, sufficient pressure should be applied to the composite layers during manufacturing. Otherwise, the separate prepreg layers constituting the part would not bind properly, and this would eventually lead to delamination under mechanical

loads. The pressure also increases part quality by allowing the entrapped air between the laminates to escape. Finally, it allows the excess resin to bleed out, resulting in higher fiber volume fractions. The pressure may be applied by several means. For example, in autoclave process it is supplied by an air compressor. In this work, the required pressure is applied by a hydraulic unit consisting of a press body and a hydraulic power unit. The hydraulic power unit actuates a Ø100x150 mm double-action hydraulic cylinder.

The pressure that should be applied for proper consolidation of AS4/8552 composite laminates is given as 7 bars by the manufacturer. The required pressure of the hydraulic pump varies according to the surface area of the part. In this study, composite plates of 100x120 mm have been manufactured. Since,

$$F = P_c . A_s \tag{5.1}$$

the required force to be exerted by the hydraulic cylinder is calculated as 8400 N. The pressure of the hydraulic pump can be calculated from the equation

$$P_{pump} = \frac{F}{A_{piston}} \tag{5.2}$$

as 10.69 bars. This pressure is supplied by the hydraulic power unit shown in Figure 5.2. The hydraulic power unit consists of a 240 bar, 10.5 cm^3/rev, pressure sensitive piston pump (1 in Figure 5.3); an elastic coupling (2); a 4 kW, 1000 rpm electric motor (4); a proportional safety valve (5); a directional control valve (6); a locking valve (7); a reducer (8); a proportional controller card (9); a temperature and level dial (10); a filling gate (11); a reservoir (12); a Ø63x200 bar pressure gage (13); and a Ø100x150 mm double-action hydraulic cylinder (14).

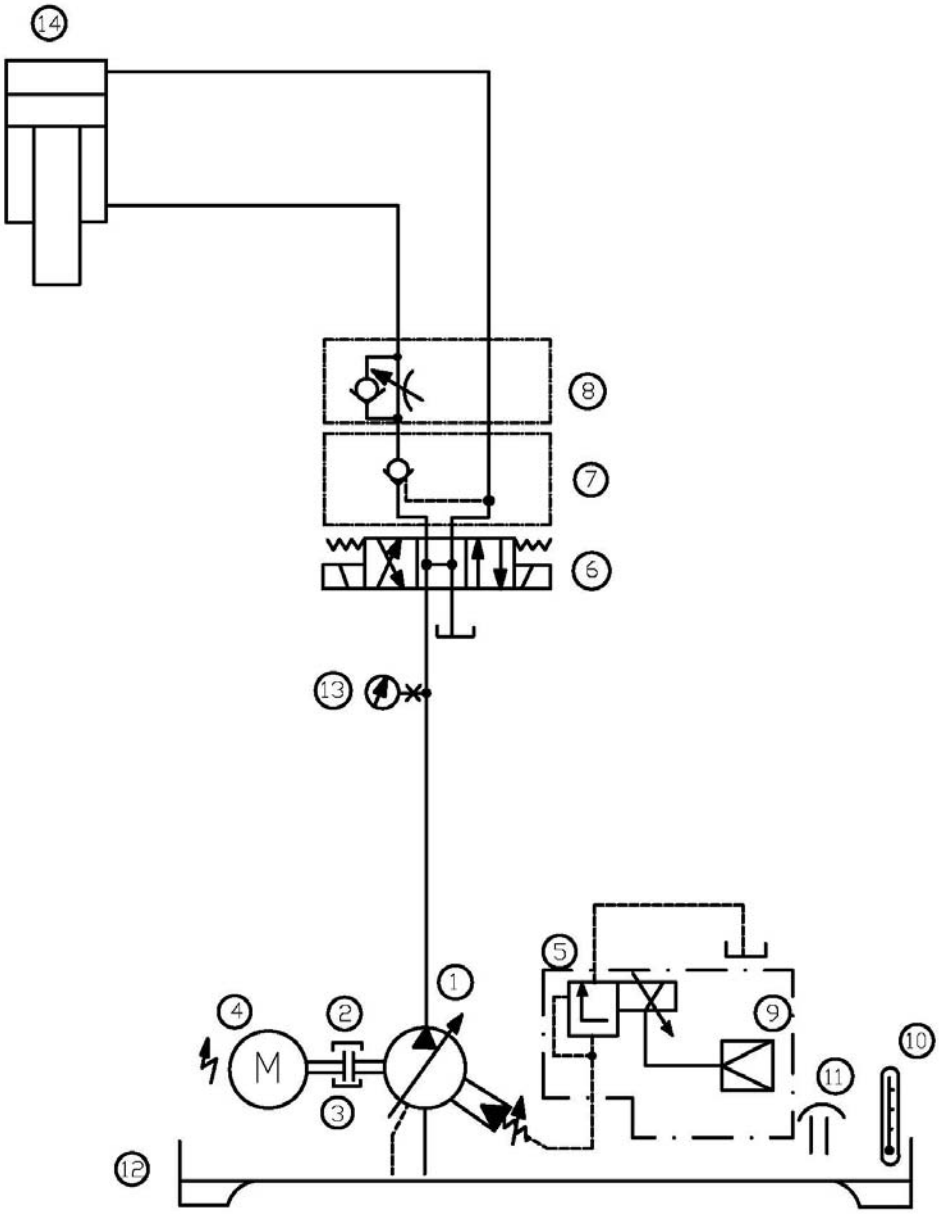

Figure 5.2. Schematic of the hydraulic circuit

5.2. Heating Molds

The heating molds are manufactured from copper to provide uniform temperature distribution. Each mold has 8x400 Watt cartridge heaters, which are close-fitted into Ø8 reamed holes. Although the effects of air cooling has not been studied in this work, cooling channels have also been included in the molds for future research (see Figure 5.3).

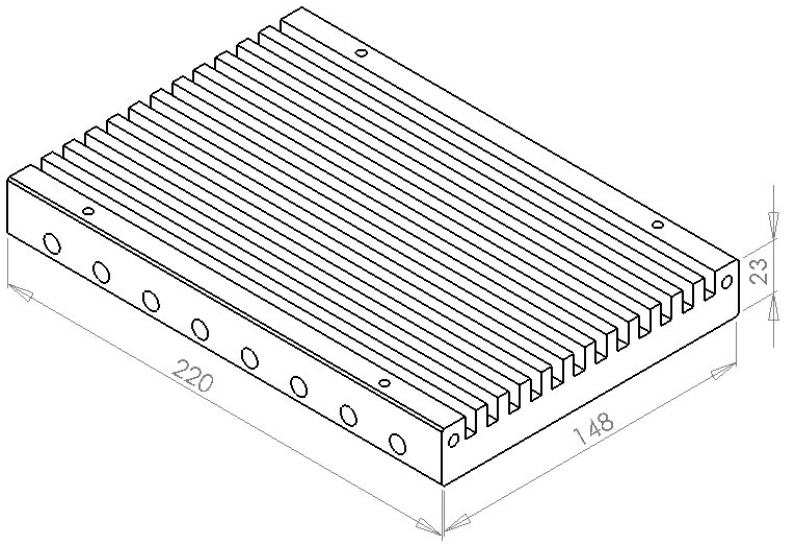

Figure 5.3. The lower heating mold

5.3. Steel Frame

A steel rectangular frame whose dimensions are 122x102x22 has been assembled to form the shape and size of the composite part. 160 layers of prepregs (0.125 mm each) are stacked in a cross-ply sequence inside this frame. Steel plates of 1 mm thickness are placed on each side of the part, and thus causing the prepreg layers to be compacted into a 20 mm thick rectangular plate. As pressure and heat are applied, the excess resin flows outside from a channel which is also used for inserting thermocouple wires (see Figure 5.4).

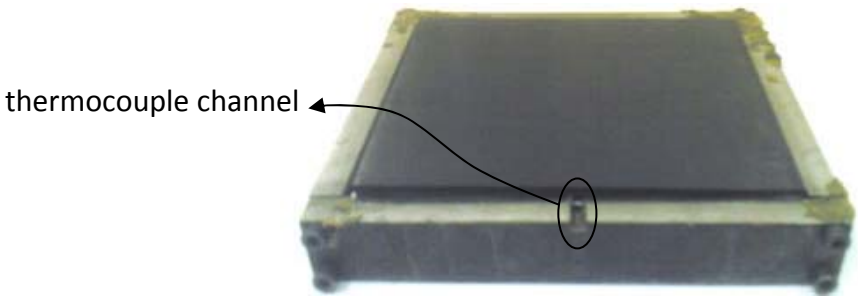

Figure 5.4**.** Steel frame

5.4. Working Principles

The heat and pressure required for the process are supplied by a hydraulic press and heating molds assembly (Figure 5.5a). The process temperature is controlled by 2 channel

PID controller unit, which has been auto-tuned and calibrated for the experiments (Figure 5.5b). The controller uses the thermocouple sensor data as the input, and generates on/off control signals. A solid state relay (Figure 5.5c) turns the heaters on/off according to these control signals. A data acquisition device (Figure 5.5d) is used for recording the temperature data coming from the thermocouples embedded inside the part.

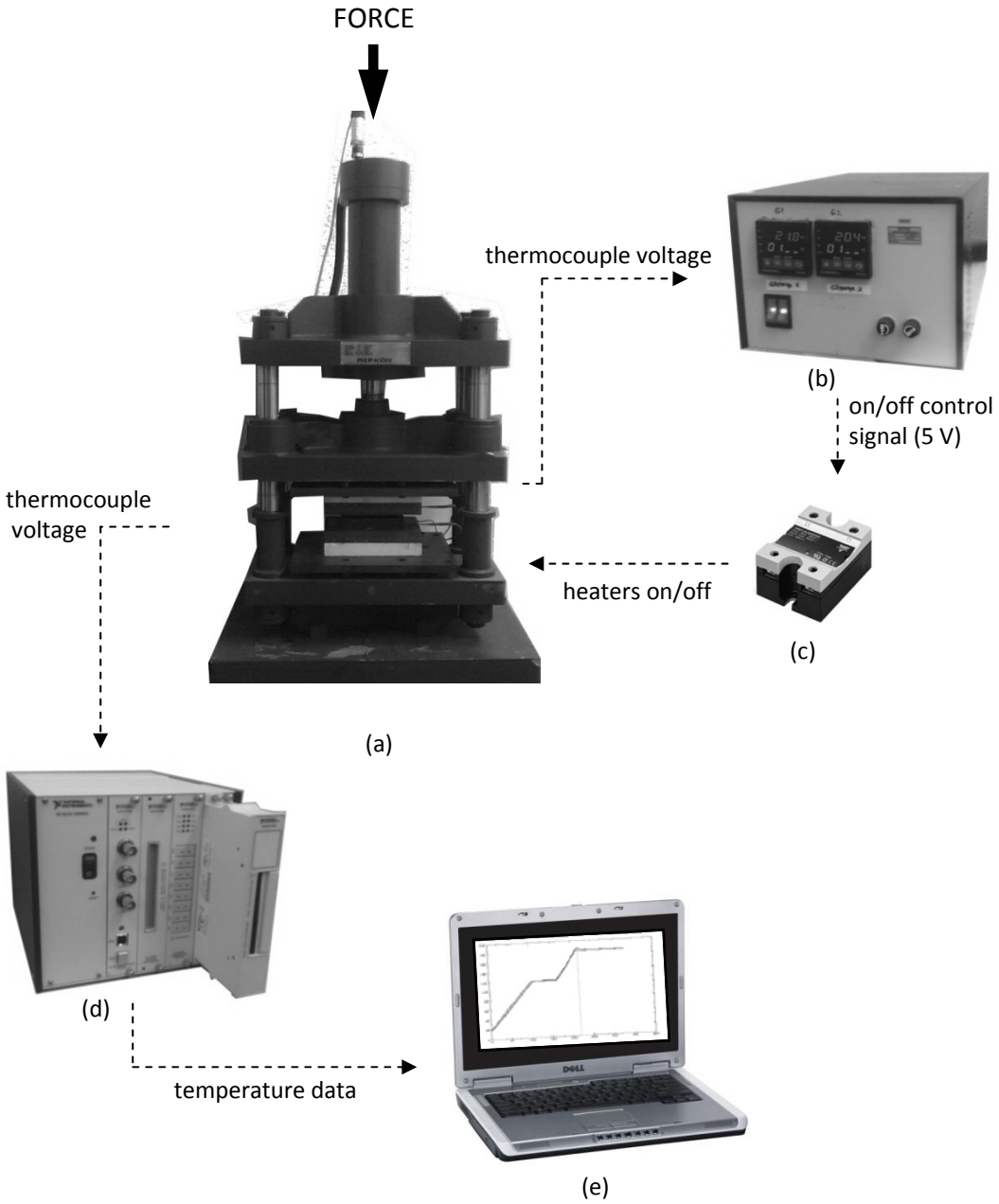

Figure 5.5. Components of the experimental setup: a) hydraulic press & mold assembly, b) 2 channel PID temperature controller, c) Solid State Relay (SSR), d) National Instruments Data Acquisition (NI-DAQ) device, e) Personal Computer (PC)

6. PID CONTROLLER DESIGN

The industrial PID controllers introduced in the previous section are not programmable for varying heating rates. Although the MRCC may be applied with those controllers, the execution of various cure cycles requires a more advanced controller. The data acquisition device used for temperature recording is suitable for this task, since it is also equipped with an analog output module.

6.1. The Basics of PID Controller

A PID controller is a structure that consists of proportional (P), integral (I), and derivative (D) gains. When dealing with a simple application, one or two of these gains may be set to zero for better performance and simplicity. For example, if the integral gain is set to zero, the controller turns into a PD controller [42]. Each gain has its characteristic pros and cons, which will be discussed in this section.

6.1.1. The Proportional Gain (K_P)

The proportional controller is the simplest controller, with the basic idea of correcting the control signal by a coefficient times the error. The coefficient is called the proportional gain, and is dependent to the system in consideration. The most important drawback of the P controller is that it is susceptible to DC error [42]. The DC error is shown in Figure 6.1.

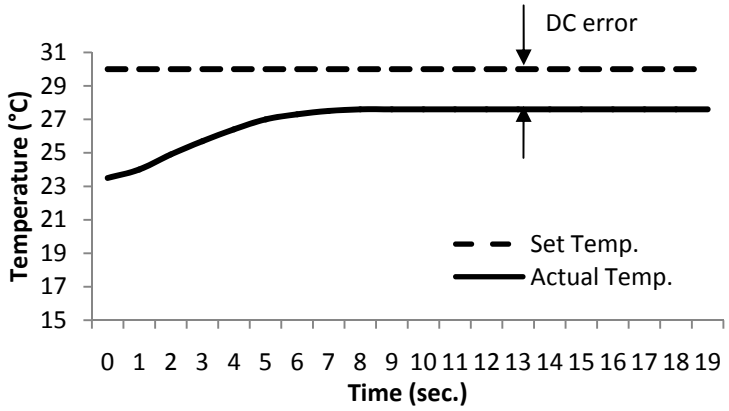

Figure 6.1. The DC error

6.1.2. The Integral Gain (K_I)

The biggest shortcoming of the P controller (the DC error) may be corrected by adding an integral gain to the system. Since the integral error will continue to cumulate at each iteration under a DC error, it will eventually compensate the proportional gain's drawback. However, a large integral gain causes overshoot (Figure 6.2), until the accumulated integral error is neutralized [42].

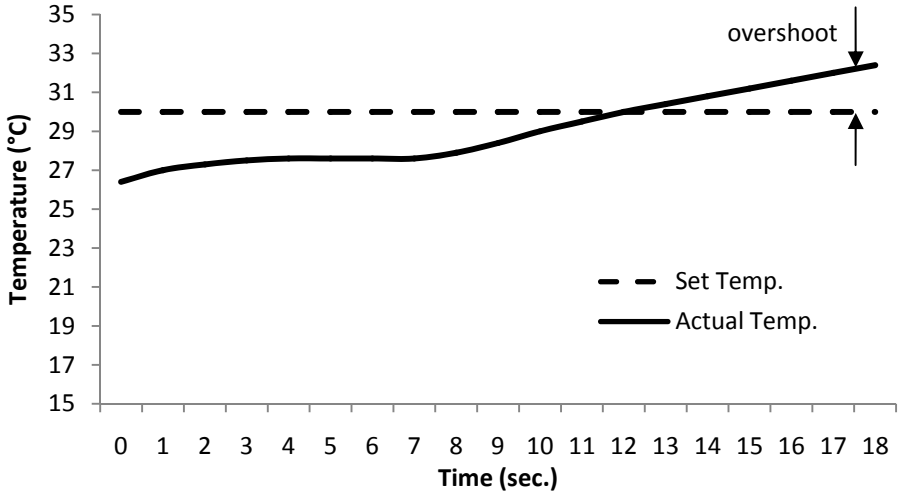

Figure 6.2. Overshoot caused by integral gain

6.1.3. The Derivative Gain (K_D)

The responsiveness of the system may be increased by adding a derivative gain to the system, which accounts for the rate of change of the error [42]. For example, in case of an overshoot caused by the integral gain, the derivative gain would realize that the system is going in the wrong direction and would try to reverse the integral gain's effect.

6.2. Tuning the PID Controller

The characteristics of a PID controller is determined by its gains. A PID controller with a high integral gain inevitably results in excessive overshoot, while a high derivative gain might cause oscillations at high frequencies. Thus, the gains of the controller should be calibrated individually for the specific purpose. This procedure is called tuning and it

might be done either manually, or automatically. The latter method is called auto-tuning. There are several methods proposed for auto-tuning, and relay auto-tuning is very popular among them. To implement this method, the system should be connected in a feedback loop shown in Figure 6.3 [43].

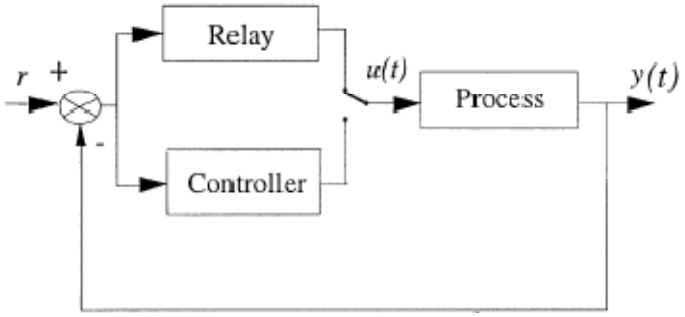

Figure 6.3. Relay feedback system [43]

To identify the ultimate period T_u and ultimate gain K_u, the relay should be controlled such that it is turned on below a certain setpoint, and turned off above it. After several switches, the system should follow an oscillation as in Figure 6.4.

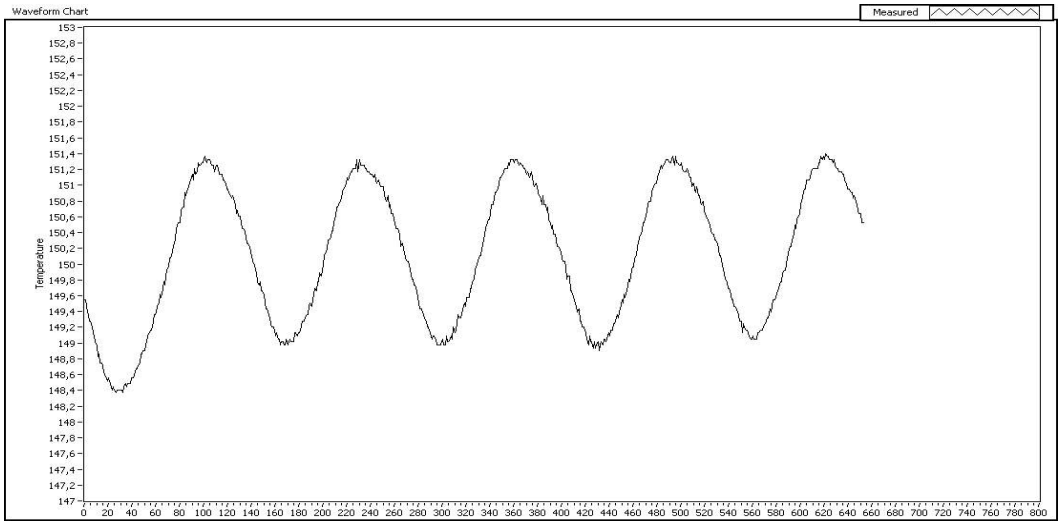

Figure 6.4. Auto-tuning of the heating system

The ultimate gain is approximately calculated by [44]

$$K_u = \frac{4d}{\pi a} \tag{6.1}$$

where d is the relay amplitude and a is amplitude of the process output.

6.3. PID Controller in LabVIEW

As stated at the beginning of this chapter, an advanced controller that may be programmed for any arbitrary curing profile is essential for this study. Such a controller has been developed using the graphical programming interface of LabVIEW 8.2.

The input for the controller is provided from the temperature channel of the data acquisition device, where the thermocouples are connected. The controller then compares the input with the temperature profile stored in an array, and calculates the duty cycle of the relay controlling the heaters. The performance of the controller may be observed from the sample heating profile shown in Figure 6.6. It is seen from the figure that the controller shows a slight oscillation, with a maximum of 0.5 °C error.

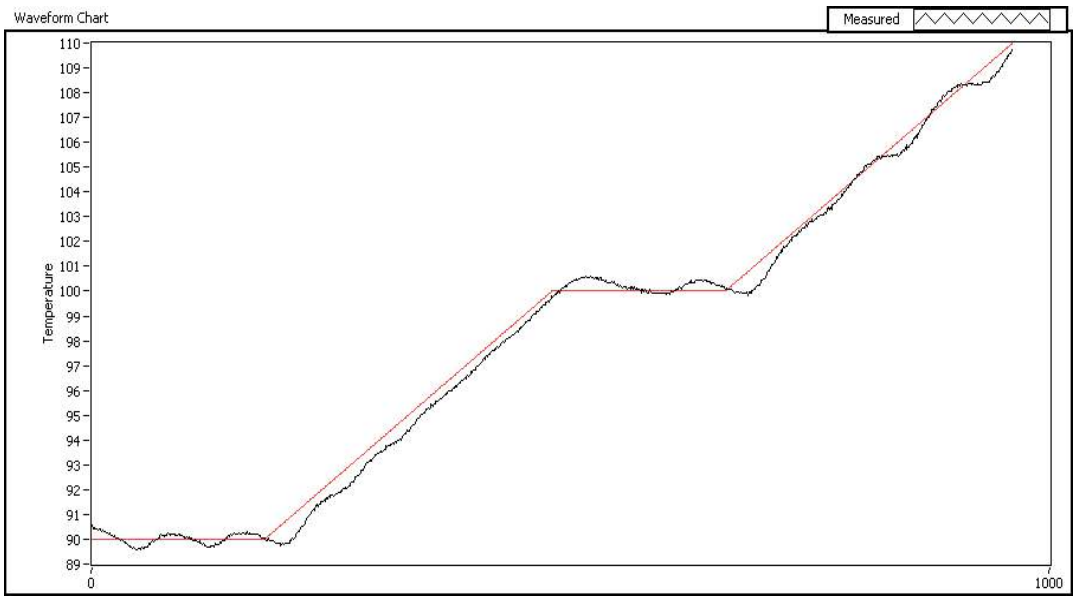

Figure 6.5. A sample performance of the controller

7. RESULTS AND DISCUSSION

In this study, a finite difference analysis has been developed to predict the temperature distribution throughout a thick-sectioned composite part. At first, the MRCC was analyzed for parts with various thicknesses, and the results were interpreted. Based on the information obtained from the analysis, an optimization algorithm that works reciprocating with the finite difference analysis has been implanted. Finally, experiments were carried out using the MRCC, and the optimized cure cycle (OCC) to verify the analysis results.

7.1. Analysis Results

A sample output of the analysis for a 20 mm thick composite part using the MRCC is shown in Figure 7.1. The dashed line represents the mold temperature (which is almost the same as the surface temperature), and the continuous line represents the temperature at the center of the part. The hatched area shows the magnitude of the exothermic reaction, and the dotted curve indicates the degree of cure (again at the center).

The reason behind the temperature gradient phenomenon can be inspected clearly in this graph. As previously discussed, at the first stage of heating, temperature at the center shows a lag because the resin serves as a thermal barrier. However, after the first dwell, as the temperature reaches a specific point, chemical reactions initiate. Note that as the degree of cure accelerates, the exothermic reaction also increases significantly, which results in a temperature gradient of about 9.68 °C at the center of the part. The aim of this study was to decrease this malignant gradient to a reasonable level.

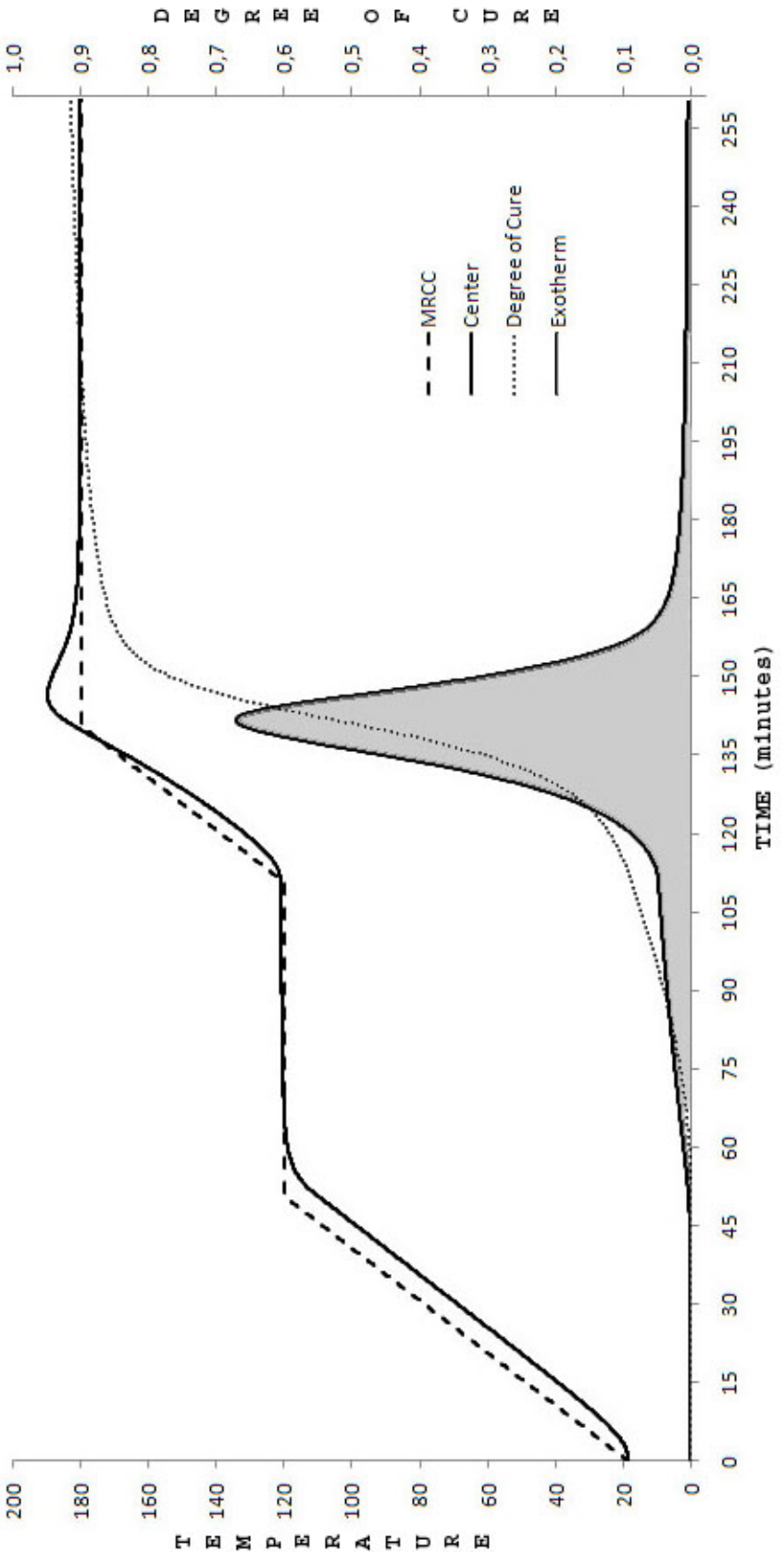

Figure 7.1. Analysis results for a 20 mm. part (MRCC)

7.2. Optimum Heating Profile

Figure 7.2 shows the optimization procedure of the second ramp phase for a 20 mm thick composite plate. The figure on the upper left is the initial set representing the MRCC, and the figure on the lower right is the optimum profile to which the program has converged. Although the MRCC has the lowest processing time, the 9.68 °C temperature gradient renders its objective function value very high, forcing the sequential simplex algorithm to search for a new path. This search continues until the shortest curing path with a maximum temperature gradient of 5 °C is found.

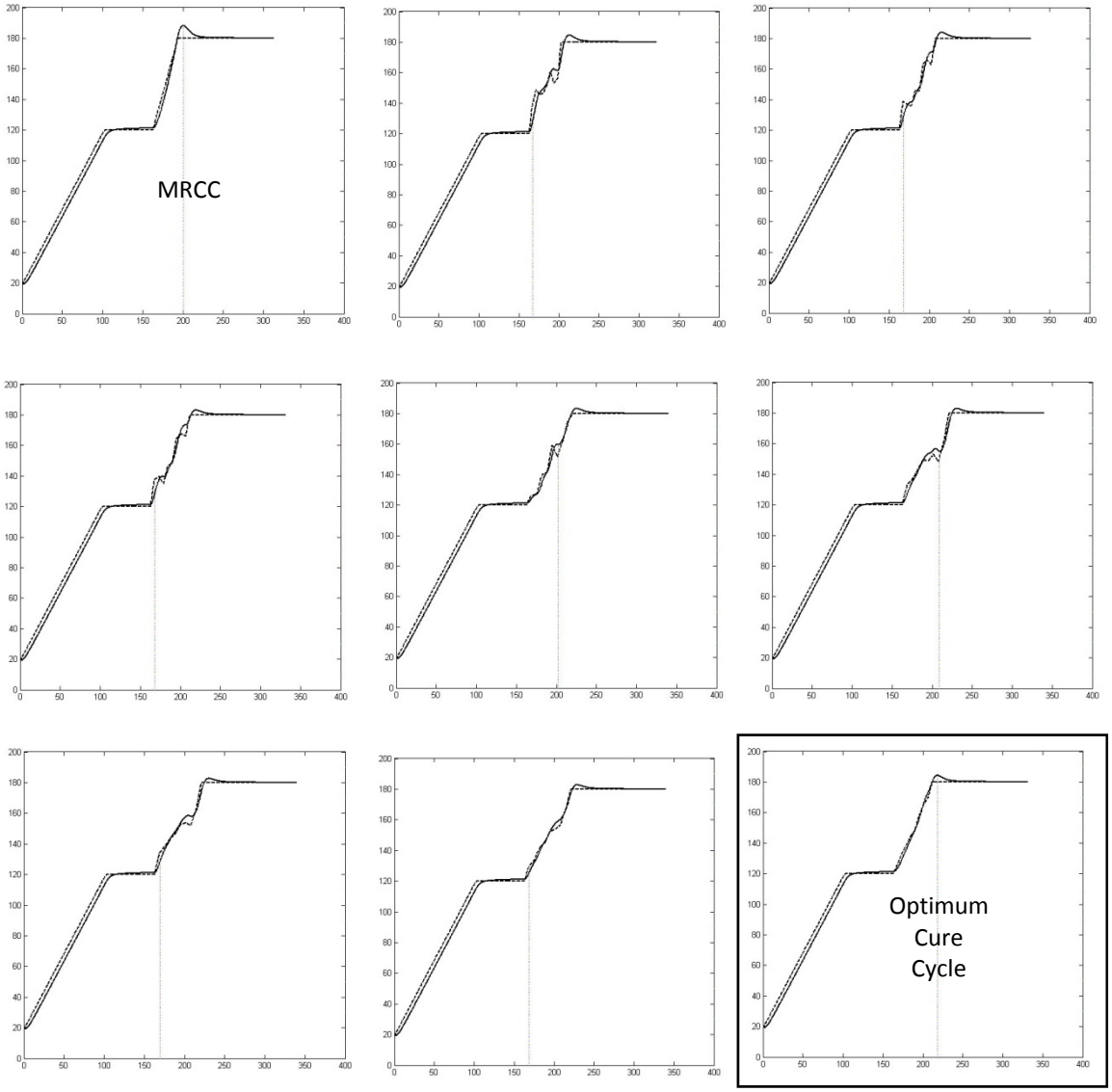

Figure 7.2. Samples from the optimization progress

Figure 7.3 shows the optimum curing profile in detail. The maximum temperature gradient decreases from 9.68 °C to 4.73 °C, while the total processing time increases from 260 minutes to 326 minutes. Although the optimal cure cycle was anticipated to follow a bumpy curve beforehand, the results gave almost a straight line. This trend may be explained by the fact that even if the increase in the surface temperature is decelerated by turning the heaters off, internal temperature still continues to rise because of the exothermic reaction. Thus, a decrease in the heating rate may even cause a sudden increase in the temperature gradient. On the other hand, increasing the heating rate over a certain rate may cause the autocatalytic reaction to accelerate, and thus again causing an increase in the temperature gradients.

However, in reality, the straight ramp converged by the optimization program might not actually be the optimal solution. First of all, because of the limit imposed on the number of design parameters, smoother curves have been implicitly eliminated. Moreover, the approach followed in this study does not account for every aspects of curing, such as residual stresses, and consolidation. The possible ameliorations will be discussed in the last chapter.

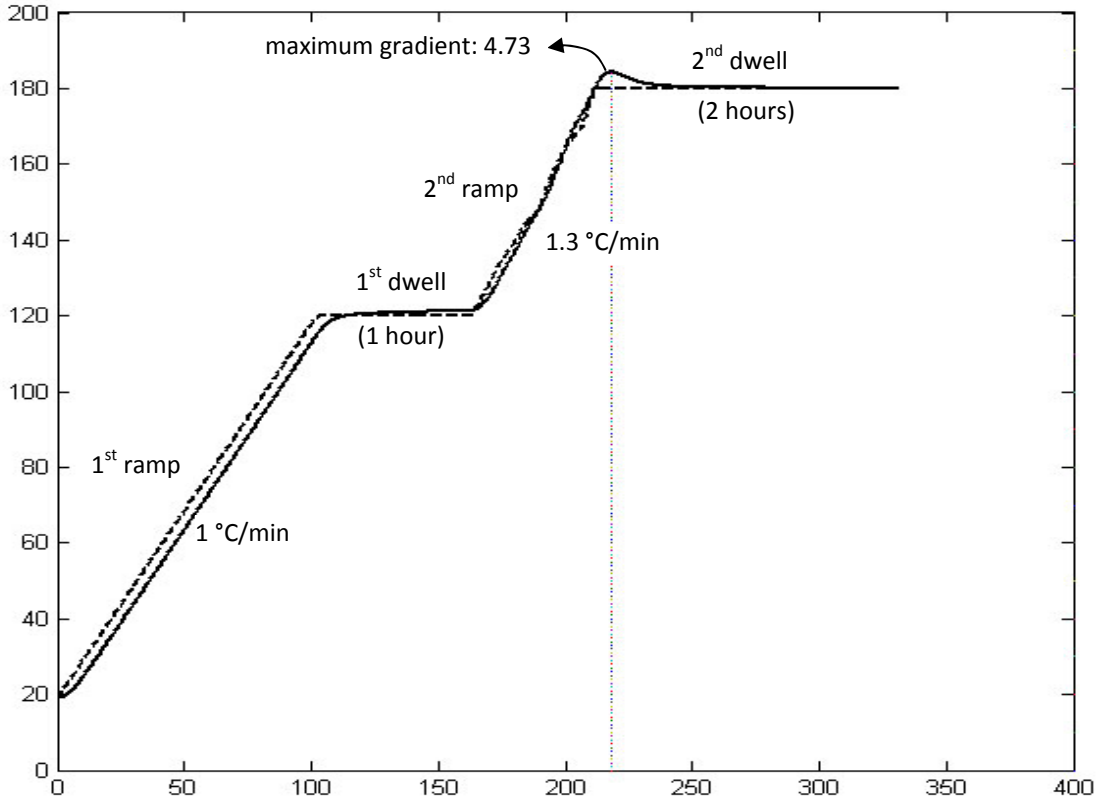

Figure 7.3. Optimum curing path for 20 mm. thickness

7.3. Experimental Results

A total of three experiments were carried out to verify the efficiency of the presented work.

7.3.1. Experiment #1

The first experiment was intended as a trial, and was conducted on a 10 mm thick part, using the MRCC (Figure 7.4). It was already predicted from the model that the maximum thermal gradient would be small (2.70 ºC). The actual gradient was 0.66 ºC higher than predicted by the model. However, the thermocouples have an accuracy of ±1 ºC, and since the temperature gradients are on the same scale, the information gathered from this experiment does not possess any significance regarding this research.

Material: AS4/8552
Part Thickness: 10 mm (80 layers)
Process: MRCC
Maximum thermal gradient (model): 2.70 ºC
Maximum thermal gradient (experiment): 3.46 ºC

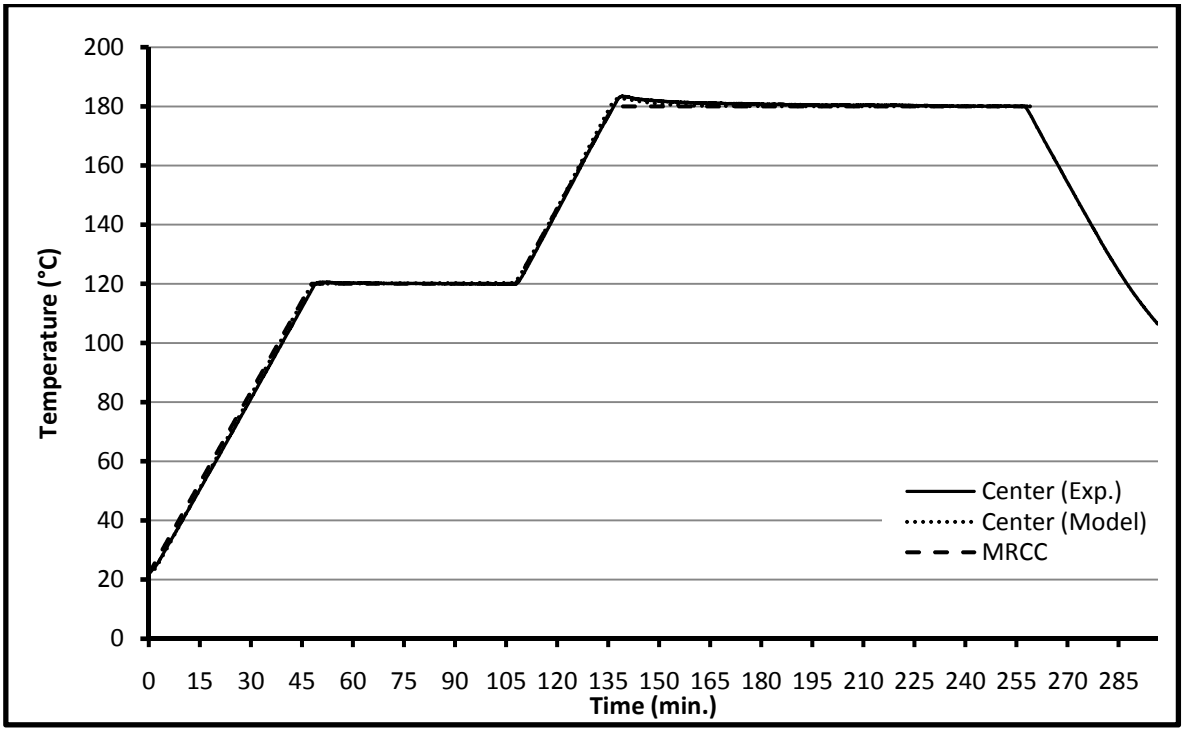

Figure 7.4. Experiment results for 10 mm. part (MRCC)

7.3.2. Experiment #2

The second experiment was conducted on a 20 mm thick part, using the MRCC (Figure 7.5). A maximum temperature gradient of 9.68 ºC was predicted by the model, and the experiment results were in good agreement with the model. The model seems to react slightly slower to temperature changes than the real part. This delay is possibly related to an accuracy problem in modeling the thermal conductivity of the composite material. There is also a constant temperature lag of about 10 ºC in the 1st ramp. It is not possible to tell without a residual stress sub-module if such a temperature difference at these temperature levels would have any detrimental effects on the part. Since cross-linking of the polymer molecules have not yet taken place in this stage of curing, no permanent defects might occur.

Material: AS4/8552
Part Thickness: 20 mm (160 layers)
Process: MRCC
Maximum thermal gradient (model): 9.68 ºC
Maximum thermal gradient (experiment): 8.69 ºC

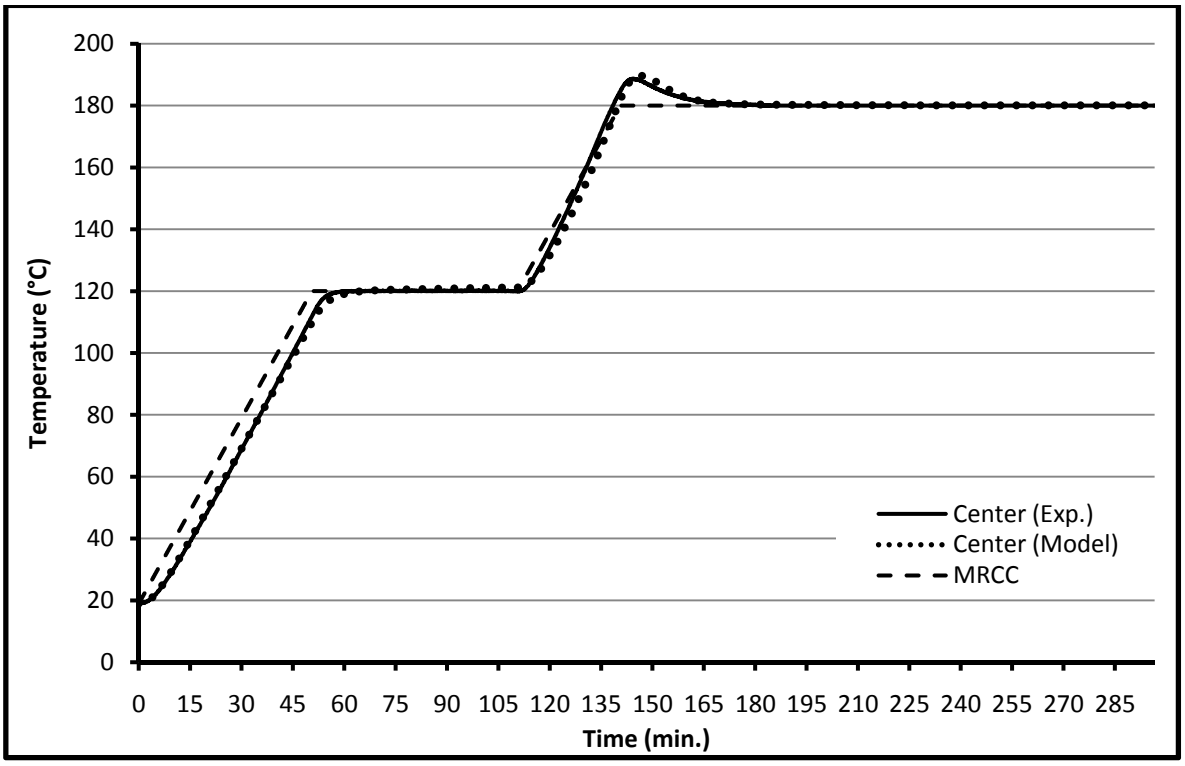

Figure 7.5. Experiment results for 20 mm. part (MRCC)

7.3.3. Experiment #3

The last experiment was conducted by using the OCC, on a 20 mm thick part (Figure 7.6). The experimental results were in very good agreement with the computer model. The slight discrepancy that has been related to thermal conductivity was again encountered in this experiment. Also, the maximum temperature gradient was 0.24 ºC lower than anticipated. The same trend may also be observed in the 2nd experiment, where the actual gradient is 0.99 ºC lower than the analysis result. This difference may be explained by the lack of the 2nd dimension in the heat transfer model. In practice, heat is also dissipated from the sides by convection as well as by conduction from the surfaces. This heat transfer which is not included in the model causes the actual temperatures to be lower than expected.

Material: AS4/8552
Part Thickness: 20 mm (160 layers)
Process: OCC
Maximum thermal gradient (model): 4.73 ºC
Maximum thermal gradient (experiment): 4.49 ºC

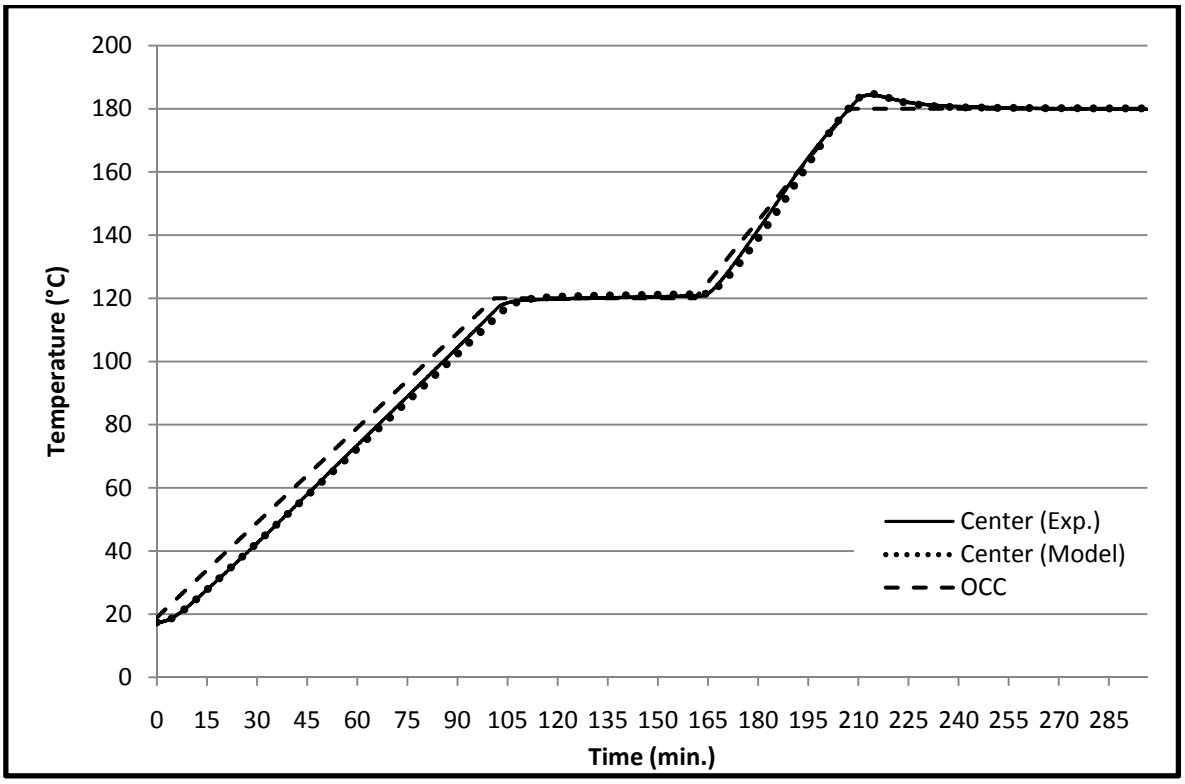

Figure 7.6. Experiment results for 20 mm. part (OCC)

8. CONCLUSIONS AND FUTURE WORK

This research covered the basics of a model-based approach for the optimal manufacturing of thick-sectioned composite parts. The heat transfer and cure kinetics of the curing phenomenon were defined by using mathematical relationships. A finite difference analysis based on these relationships was developed for predicting the temperature distribution and degree of cure for any given process parameters. This finite difference algorithm was then embedded in an optimization algorithm; namely sequential simplex method. Finally, experiments were conducted to verify the results obtained from the analysis. The proposed approach was successful at reducing the high temperature gradients encountered in thick-sectioned composite parts. However, other factors such as consolidation and residual stresses were left out of the scope of this study.

Although the work presented here does not possess all the aspects necessary for an industrial application, it constitutes a solid base for further research. By adding new sub-models to the mathematical model, and new constraints to the optimization process, the manufacturing of better parts in shorter processing times may be achieved. The potential ameliorations include:

- Adding a residual stress sub-model, and including residual stress minimization in the optimization problem.
- Adding of a resin flow sub-model, and including void minimization in the optimization problem.
- Using a 2-D heat transfer model that accounts for the convection heat transfer from the sides.
- Development of a 3-D model to allow the analysis of parts with arbitrary shapes.
- Implementation of an observer for temperature estimations, and thus eliminating the embedded thermocouples that compromise part strength.
- Replacing the PID controller with a predictive control algorithm to further reduce the temperature gradients.
- Adding cooling capability to the setup.

Table 8.1 sorts the individual phases in curing according to their process times, and Figure 8.1 shows the magnitude of these values in a chart. It is evident that the highest percentage in the whole process belongs to the dwell periods. Aiming to reduce the length of these periods would be a very efficient approach. As previously stated, the 1st dwell is intended for the proper consolidation of the composite. The addition of a resin flow sub-model would enable the optimization of the 1st dwell phase, and merging the dwell phase with the heating ramp would be possible.

A careful observation of Figure 7.1 reveals the fact that curing of the resin almost reaches its limit after 1 hour of dwell at the cure temperature. Adding degree of cure as another objective to the optimization problem would result in shorter processing times, while the strength of the composite would remain almost the same.

Table 8.1. Process times of individual phases

	1st ramp	**1st dwell**	**2nd ramp**	**2nd dwell**	**TOTAL**
MRCC	50 min.	60 min.	30 min.	120 min.	260 min.
Optimized	100 min.	60 min.	46 min.	120 min.	326 min.

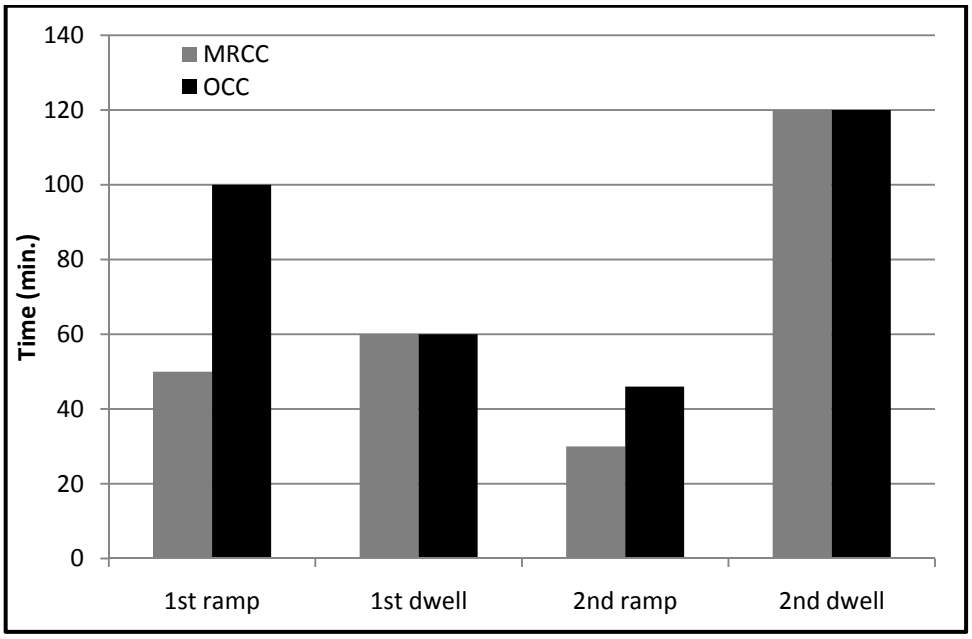

Figure 8.1. Process times for individual phases

REFERENCES

1. Mazumdar, S.K., *Composites Manufacturing*, CRC Press, Florida, 2002.

2. Prime, R.B., *Thermal Characterization of Polymer Materials*, Academic Press, New York, 1982.

3. Parthasarathy, S., Mantell, S.C., and Stelson, K.A., "Estimation, Control, and Optimization of Curing in Thick-Sectioned Composite Parts", *Journal of Dynamic Systems, Measurement, and Control*, Vol. 126, pp. 824-833, December 2004.

4. Bogetti, T.A., and Gillespie, J.W., "Two-Dimensional Cure Simulation of Thick Thermosetting Composites", *Journal of Composite Materials*, Vol. 25, pp. 239-273, March 1991.

5. Jiang, Y., and Hoa, S.V., "A Novel Method for the Manufacturing of Thick Composites", *Journal of Composite Materials*, Vol. 40, pp. 433-453, 2006.

6. Michaud, D.J., Beris, A.N., and Dhurjati, P.S., "Curing Behavior of Thick-Sectioned RTM Composites", *Journal of Composite Materials*, Vol. 32, pp. 1273-1296, 1998.

7. Kim, J. S., and Lee, D.G., "Development of an Autoclave Cure Cycle with Cooling and Reheating Steps for Thick Thermoset Composite Laminates," *Journal of Composite Materials*, Vol. 31, pp. 2264–2282, 1997.

8. Servais, R.A., Lee, C.W. and Browning, C.E., "Intelligent Processing of Composite Materials", *SAMPE Journal*, Vol. 22, pp. 14-18, 1986.

9. Loos, A.C., and Springer, G.S., "Curing of Epoxy Matrix Composites", *Journal of Composite Materials*, Vol. 17, pp. 135-169, March 1983.

10. Lee, W.I., and Springer, G.S., "Microwave Curing of Composites", *Journal of Composite Materials*, Vol. 18, pp. 387-409, July 1984.

11. Oh, J.H., and Lee, D.G., “Cure Cycle for Thick Glass/Epoxy Composite Laminates”, *Journal of Composite Materials*, Vol. 36, pp. 19-45, 2002.

12. Yang Z. L., and Lee S., “Heating Cycle Design for Thick Composite Laminates Using Curing Processes for Thin Laminates”, *Journal of Reinforced Plastics and Composites*, Vol. 21, pp. 1543-1560, 2002.

13. Johnston, A., Hubert, P., and Poursartip, A., *A Review of Process-Induced Stress and Deformation Modelling in Fibre-Reinforced Composite Structures*, The University of British Columbia, 1993.

14. Bogetti, T.A., and Gillespie, J.W., “Process-Induced Stress and Deformation in Thick-Section Thermoset Composite Laminates”, *Journal of Composite Materials*, Vol. 26, pp. 626-660, 1992.

15. Ciriscioli, P.R., Springer, G.S., and Lee, W.I., “An Expert System for Autoclave Curing of Composites”, *Journal of Composite Materials*, Vol. 25, pp. 1542–1587, December 1991.

16. Pillai, V.K., Beris, A.N., and Dhurjati, P.S., “Implementation of Model-Based Optimal Temperature Profiles for Autoclave Curing of Composites Using a Knowledge-Based System”, *Ind. Eng. Chem. Res*., Vol. 33, pp. 2443-2452, 1994.

17. White, S.R., and Kim., Y.K., “Staged Curing of Composite Materials”, *Composites Part A,* Vol. 27A, No. 3, pp. 219-227, 1996.

18. Reuss, J.D., Fowler, A.J., Kim, Y.K., and Lewis, A., “Manufacture of Thick Cross-Section Composites Using a Pre-Catalyzed Fabric Technique”, *Journal of Composite Materials*, Vol. 36, pp. 1367-1379, 2002.

19. Hay, J.N., and O’Gara, P., “Recent Developments in Thermoset Curing Methods”, *Proc. IMechE*, Vol. 220, pp. 187-195, 2006.

20. Ramakrishnan, B., Zhu, L., and Pitchumani, R., "Curing of Composites Using Internal Resistive Heating", *Journal of Manufacturing Science and Engineering*, Vol. 122, pp. 124-131, February 2000.

21. Park, H.C., and Lee, S.W., "Cure Simulation of Thick Composite Structures Using the Finite Element Method", *Journal of Composite Materials*, Vol. 35, pp. 188-201, 2001.

22. Choi, M.A., Lee, M.H., Chang. J., and Lee. S.J., "Three-Dimensional Simulations of the Curing Step in the Resin Transfer Molding Process", *Polymer Composites*, Vol. 20, pp. 543-552, August 1999.

23. Michaud, D.J., Beris, A.N., and Dhurjati P.S., "Thick-Sectioned RTM Composite Manufacturing: Part I – In Situ Cure Model Parameter Identification and Sensing", *Journal of Composite Materials*, Vol. 36, pp. 1175-1200, 2002.

24. Pantelis, N.G., "Towards the Dynamic Optimisation for the Cure Control of Thermoset-Matrix Composite Materials", *Composites Science and Technology*, Vol. 65, pp. 1254-1263, 2005.

25. Mason, K.F., "Monitoring the Cure Itself", *High-Performance Composites*, September 2006.

26. Antonucci, V., Giordano, M., Cusano, A., Nasser, J., and Nicolais, L., "Real Time Monitoring of Cure and Gelification of a Thermoset Matrix", *Composites Science and Technology*, Vol. 66, pp. 3273-3280, 2006.

27. Garnier, B., and Sommier, A., "Thermal Property Measurements During Curing of Thermoset Resins Using Steady Periodic Conditions", *Journal of Reinforced Plastics and Composites,* Vol. 21, No. 13, pp. 1193-1203, 2002.

28. Johnston, A.A., *An Integrated Model of the Development of Process-Induced Deformation in Autoclave Processing of Composite Structures*, Ph.D. Thesis, The University of British Columbia, 1997.

29. Scott, E.P., “Determination of Kinetic Parameters Associated with the Curing of Thermoset Resins Using Dielectric and DSC Data", *Composites: Design, Manufacture, and Application, ICCM/VIII*, pp. 100-110, 1991.

30. Kenny, J.M., Trivisano, A., and Berglund L.A., "Chemorheological and Dielectric Behavior of the Epoxy Matrix in a Carbon Fiber Prepreg", *SAMPE Journal* 27 (2), pp. 39-45, 1991.

31. Lee, S.N., Chiu, M.T., and Lin, H.S., "Kinetic Model for the Curing Reaction of a Tetraglycidyl Diamino Diphenyl Methane/Diamino Diphenyl Sulfone (TGDDM/DDS) Epoxy Resin System", *Polymer Engineering and Science*, 32 (15), pp. 1037-1046, 1992.

32. Cole, K.C., Hechler, J.J., Noël D., “A New Approach to Modeling the Cure Kinetics of Epoxy Amine Thermosetting Resins. 2. Application to a Typical System Based on Bis[(4-diglycidylamino)phenyl]methane and Bis(4-aminophenyl) Sulphone”, *Macromolecules*, 24 (11), pp. 3098–110, 1991.

33. Ersoy, N., Potter, K., Wisnom, M.R., Clegg, M.J., “Development of Spring-in Angle During Cure of a Thermosetting Composite”, *Composites Part A*, Vol. 36, pp. 1700-1706, 2005.

34. Springer, G.S., and Tsai, S.W., “Thermal Conductivities of Unidirectional Materials, *Journal of Composite Materials*, Vol. 1, pp. 166-173, 1967.

35. Hoffman, J.D., *Numerical Methods for Engineers and Scientists*, McGraw-Hill, Inc., New York, 1993.

36. Parthasarathy, S., *Real-Time Control and Optimization of Curing in Thick Sectioned Thermoset Composites*, Ph.D. Thesis, University of Minnesota, 2002.

37. Arpacı, V.S., *Conduction Heat Transfer*, Addison-Wesley, Massachusetts, 1966.

38. Haftka, R.T., and Gürdal, Z., *Elements of Structural Optimization*, Kluwer Academic Publishers, Dordrecht, 1992.

39. Nelder, J.A., and Mead, R., "A Simplex Method for Function Minimization", *The Computer Journal*, Vol. 7(4), pp. 308-313, 1965.

40. Spendley, W., Hext, G.R., and Himsworth, F.R., "Sequential Application of Simplex Designs in Optimisation and Evolutionary Operation", *Technometrics*, Vol. 4(4), pp. 441-461, 1962.

41. Sönmez, F.Ö., and Eyol, E., "Optimal Post-manufacturing Cooling Paths for Thermoplastic Composites", *Composites Part A*, vol. 33, pp. 301-314, 2002.

42. Ellis, G., *Control System Design Guide*, Elsevier Academic Press, USA, 2004.

43. Hang, C.C., Astrom K.J., and Wang, Q.G., "Relay Feedback Auto-tuning of Process Controllers – A Tutorial Review", *Journal of Process Control*, vol. 12, pp. 143-162, 2002.

44. Hang, C.C., Astrom, K.J., and Ho, W.K., "Refinements of the Ziegler–Nichols Tuning Formula", *IEE Proceedings-D*, vol. 138 (2), pp. 111–118, 1991.